JGR Earth Surface

RESEARCH ARTICLE
10.1029/2023JF007244

Special Section:
Controls and Biasing Factors in Sediment Generation, Routing, and Provenance: Models, Methods, and Case Studies

Detrital Garnet Geochronology by In Situ U-Pb and Lu-Hf Analysis: A Case Study From the European Alps

Chris Mark[1,2], Gary O'Sullivan[1], Stijn Glorie[3], Alexander Simpson[3], Sergio Andò[4], Marta Barbarano[4], Laura Stutenbecker[5], J. Stephen Daly[1,6], and Sarah Gilbert[7]

[1]UCD School of Earth Sciences, UCD Earth Institute, University College Dublin, Dublin, Ireland, [2]Now at Department of Geosciences, Swedish Museum of Natural History, Stockholm, Sweden, [3]Department of Earth Sciences, University of Adelaide, Adelaide, SA, Australia, [4]Department of Earth and Environmental Sciences, Università di Milano-Bicocca, Milan, Italy, [5]Institute of Geology and Paleontology, Westfälische Wilhelms-Universität Münster, Münster, Germany, [6]Science Foundation Ireland Research Centre in Applied Geosciences (iCRAG), University College Dublin, Dublin, Ireland, [7]Adelaide Microscopy, University of Adelaide, Adelaide, SA, Australia

Abstract Detrital geochronology employing the widely-used zircon U-Pb proxy is biased toward igneous events and metamorphic anatexis; additionally, zircon is highly refractory and frequently polycyclic. Garnet, a rock-forming and thus commonly occurring mineral, is predominantly metamorphic and much less refractory. Here, we report in situ U-Pb and Lu-Hf ages from detrital garnet hosted in ancient and modern sediments of the European Alps. Both geochronometers are biased toward the most recent garnet-crystallizing metamorphic event in the source area, with fewer inherited ages. This likely reflects efficient removal of inherited garnet during diagenesis and metamorphism, and is in contrast to detrital zircon, apatite, and rutile U-Pb data, which largely record pre-Alpine ages. Neither the U-Pb nor Lu-Hf system in garnet exhibits a relationship between age recovery and composition. However, the Lu-Hf system in garnet yields significantly better age recovery than the U-Pb system. Estimated initial $^{238}U/^{206}Pb_c$ values at the time of crystallization are near unity, suggesting that garnet does not significantly partition U from Pb during crystallization, at least for the generally almandine-rich garnets analyzed in this study. Hence, Lu-Hf geochronology of detrital garnet offers an effective method to detect and date the most recent phase of mid-grade metamorphism in sub-anatectic source areas, in which detrital zircon U-Pb analysis may be of less utility.

Plain Language Summary Mountain ranges are characterized by rapid changes in their constituent rocks as these undergo metamorphism to adjust to increasing pressure and temperature during tectonic burial. These metamorphic processes drive mineral crystallization. Once cooled, each mineral acts as a geochemical reservoir isolated from the surrounding environment. Therefore, if a mineral has incorporated a radioactive isotope during crystallization, it can be dated to constrain the timings and rates of metamorphism. As erosion ultimately converts crystalline bedrock to sediment, the geological histories of these processes are preserved in the sediment shed during erosion. Consequently, these histories can be read from sedimentary rocks in adjacent sedimentary basins. Minerals traditionally used to study the sources of these sediments, such as zircons, largely grow from molten rock rather than during metamorphism, and are tough enough to be recycled through multiple tectonic events. The mineral garnet more commonly grows under metamorphic conditions and is thus more effective at directly recording the most recent phases of significant mountain building. Here, we present uranium-lead and lutetium-hafnium ages of garnet in modern and ancient sediment from the Alps. We show that garnet preferentially records Alpine events and is thus suitable for provenance studies targeting the most recent mountain building event.

Key Points:

- Detrital garnet U-Pb and Lu-Hf ages preferentially record the most recent metamorphic event in the source area
- Both systems are less refractory than alternative detrital U-Pb geochronometers
- Age recovery for Lu-Hf in garnet is considerably better than for U-Pb

Supporting Information:

Supporting Information may be found in the online version of this article.

Correspondence to:
C. Mark,
chris.mark@nrm.se

Citation:
Mark, C., O'Sullivan, G., Glorie, S., Simpson, A., Andò, S., Barbarano, M., et al. (2023). Detrital garnet geochronology by in situ U-Pb and Lu-Hf analysis: A case study from the European Alps. *Journal of Geophysical Research: Earth Surface*, *128*, e2023JF007244. https://doi.org/10.1029/2023JF007244

Received 5 MAY 2023
Accepted 5 SEP 2023

1. Introduction

1.1. The Utility of Detrital Garnet in Sedimentary Provenance Analysis

Detrital geochronology is a powerful tool for interrogating the sedimentary archive of paleo-hinterland tectonic, metamorphic, and climatic processes, and can also be applied to modern river sediment as a first-pass tool to establish regional bedrock ages (e.g., Ledent et al., 1964; Machado & Gauthier, 1996; Najman, 2006; von Eynatten & Dunkl, 2012). The zircon U-Pb detrital geochronometer has seen widespread adoption in provenance analysis (3,626 of 4,471 results for the search term *detrital geochronology* also contain the term *zircon U-Pb*; Clarivate Analytics Web of Science). However, zircon fertility is strongly biased toward intermediate to felsic

source rocks (Boehnke et al., 2013). Moreover, zircon neocrystallization is volumetrically limited in metamorphic terranes which do not achieve anatexis (e.g., Moecher & Samson, 2006), and is typically restricted to rim overgrowths which are vulnerable to mechanical destruction during fluvial transport, and which are also challenging to detect and analyze (e.g., Campbell et al., 2005).

Therefore, it is desirable to develop complementary provenance tools to identify metamorphic source rocks in the detrital record (Zack et al., 2011). Garnet group minerals are rock-forming in several common metamorphic lithologies and are also present as accessory minerals in a wide range of igneous and metamorphic rocks. Garnet is therefore a common constituent of clastic detritus from orogens. Here and throughout, we use the term *garnet* as a synonym for garnet group silicates in the garnet supergroup. These have the general formula $X_3Y_2Z_3O_{12}$ in which the *Z*-site is occupied by Si; the 14 known end members of this complex solid solution include the geologically common varieties almandine $Fe_3Al_2(SiO_4)_3$, andradite $Ca_3Fe_2(SiO_4)_3$, grossular $Ca_3Al_2(SiO_4)_3$, spessartine $Mn_3Al_2(SiO_4)_3$, pyrope $Mg_3Al_2(SiO_4)_3$, and uvarovite $Ca_3Cr_2(SiO_4)_3$ (Grew et al., 2013).

The wide range of documented stoichiometry, and potential for correlation to source rock type, has resulted in extensive use of garnet composition as a detrital provenance tool (Connally, 1964; Morton, 1985; Schönig et al., 2021; Stutenbecker et al., 2017; Suggate & Hall, 2014). Importantly, the broad P-T stability range of garnet in most bulk rock compositions means that neocrystalline garnet is shed to the sediment routing network during almost every orogenic exhumational phase, beginning with epidote-garnet dominated heavy mineral assemblages from upper-greenschist-facies-grade metasedimentary cover units, through gneissose hornblende-garnet-epidote-aluminosilicate suites, culminating in debris from garnet-cordierite bearing leucogranites generated by anatexis (Andò et al., 2013; Garzanti, Resentini, et al., 2010). Garnet group minerals average 13% of the heavy mineral fraction in the bedload of rivers draining major modern orogens where sediment production is dominated by rapid exhumation of metamorphic crystalline bedrock, including the Po, Ganges-Brahmaputra, and Indus (Garzanti & Andò, 2007; Garzanti et al., 2005; Garzanti, Andò, et al., 2010; Garzanti, Resentini, et al., 2010). In rivers draining tectonically quiescent continental interiors characterized by widespread ancient sedimentary cover, the garnet fraction averages just 3%, including the Amazon, Congo, Mississippi, Nile, and Zambezi (do Nascimento et al., 2015; Garzanti et al., 2015, 2019, 2021; Mange & Otvos, 2005).

Despite the abundance of garnet in recent surficial sediments, it is only moderately stable during diagenesis. Studies of Cenozoic-Mesozoic depocenters in the North Sea, Nile Delta, Bay of Bengal and Gulf of Mexico indicate that near-complete dissolution of sand-grade garnet occurs at burial depths of 4–5 km (Andò et al., 2012; Garzanti et al., 2018; Milliken, 2007; Morton & Hallsworth, 2007). Garnet is also rapidly destroyed by prolonged residence in soils (Andò et al., 2012; Velbel, 1984). As a result, garnet is considerably less refractory than other commonly-used detrital U-Pb geochronometers, including zircon, rutile, apatite, but more so than titanite, which is typically removed at 3–4 km burial depths (Andò et al., 2012; Garzanti et al., 2018; Morton & Hallsworth, 2007). Recycling of detrital garnet into younger orogens is thus expected to be rare, although it has been reported (Manzotti & Ballèvre, 2013). Garnet is also commonly eliminated from metasediment during the early stages of metamorphism (Cave et al., 2015), but the preservation of inherited garnet retained in polycyclic crystalline bedrock has also been reported (Argles et al., 1999; Simpson et al., 2023; Walker et al., 2021). Significantly, a compositional control on garnet diagenetic stability has been documented, with a decrease in the Ca content of bulk garnet separates with burial depth and an increase in Fe content (Morton & Hallsworth, 2007). As Mn and Mg contents in that example remained unchanged, this could indicate higher diagenetic vulnerability of grossular- and uvarovite-rich garnets.

1.2. Garnet Geochronology

In crystalline bedrock, garnet is datable using the Rb-Sr, Sm-Nd, Lu-Hf, and U-Pb radioisotope systems. As with many geochronometers, the garnet host seldom completely excludes the daughter element during crystal growth; therefore, the isotopic composition of the initial daughter component must be corrected during age calculation, normally by the isochron method (Nicolaysen, 1961). Garnet typically has extremely low Rb/Sr ratios, so the $^{87}Rb/^{86}Sr$ age is calculated as a model age from $^{87}Sr/^{86}Sr$, requiring assumptions regarding matrix Rb/Sr during garnet growth which cannot easily be verified in a detrital context (Christensen et al., 1989). Typical $^{147}Sm/^{144}Nd$ ratios, while higher than $^{87}Rb/^{86}Sr$, are also low (typically <3 except in highly fractionated rocks such as pegmatites; Thöni, 2003). Coupled with the long half-life of ^{147}Sm, analysis of a co-crystallizing phase with lower initial Sm/Nd is required to anchor the Sm-Nd isochrons (e.g., Baxter & Scherer, 2013). Low Sm/Nd

and slow radiogenic ingrowth probably renders impractical the use of detrital single-garnet Sm-Nd analyses coupled with initial $^{143}Nd/^{144}Nd$ estimates obtained from Nd isotope terrestrial evolution models (e.g., DePaolo & Wasserburg, 1976). This hinders application of the Sm-Nd technique to detrital studies. Although co-analysis of either bulk sediment hosting the detrital grains (Oliver et al., 2000) or garnet-hosted inclusions have been employed to allow the construction of single-grain isochrons (Maneiro et al., 2019), both methods are somewhat laborious.

In contrast, initial $^{176}Lu/^{177}Hf$ in garnet is typically high (Duchêne et al., 1997) and the terrestrial range of initial Hf isotopic compositions is small (Vervoort et al., 1999), such that correction for initial Hf becomes relatively trivial at the level of precision typically required for detrital studies (Simpson et al., 2021). Empirical and experimental studies show that the initial U/Pb ratio in garnet can be high (Haack & Gramse, 1972; Hauri et al., 1994); moreover, the relatively predictable isotopic evolution of crustal Pb (Stacey & Kramers, 1975) facilitates the correction of single-analysis U-Pb ages for initial Pb using the same approach typically employed for detrital analysis of other common-Pb hosting phases (e.g., Chew et al., 2020). Additionally, the half-lives of ^{176}Lu and $^{238,235}U$ are shorter than for ^{87}Rb and ^{147}Sm, leading to faster radiogenic ingrowth. Both techniques are therefore suitable in principle for detrital single-grain analysis.

Lu-Hf dating of garnet, initially by solution and now also by in situ methods, is uncontroversial (Duchêne et al., 1997; Simpson et al., 2021). In contrast, U-Pb dating of garnet, despite having a longer history (Burton et al., 1995; Mezger et al., 1989), has been the subject of debate centered around whether U is hosted in the garnet lattice, or as inclusions which may be inherited (DeWolf et al., 1996). However, multiple lines of evidence support the incorporation of U in garnet as a trace element, although the mechanisms of incorporation and extent of possible stoichiometric controls remain unclear. Dissolution of bulk detrital garnet separates obtained from modern bedload of the Brahmaputra river indicated an average U content of 3.5 μg/g, although co-dissolution of U-hosting inclusions cannot be excluded (Garçon et al., 2014). In situ empirical studies by etching of spontaneous fission tracks or ion microprobe analysis have demonstrated homogeneously-distributed U in garnet up to several hundred μg/g (Haack & Gramse, 1972; Smith et al., 2004), with andradite and spessartine typically containing higher U concentrations than almandine, pyrope, or grossular. Experimental synthesis of pyrope-rich and pyrope-grossular garnet from silicate melts yields U concentrations up to 60 μg/g; garnet/melt partitioning coefficients are non-zero, demonstrating that garnet does not completely reject U during formation (Hauri et al., 1994; Van Westrenen et al., 1999).

In addition to experimental studies documenting the presence of U in the lattice, mineralogical mechanisms for U-incorporation have also been articulated. Structural modeling of ferrite garnet, in which the *Z*-site Si is partially replaced by Fe, indicates that the resulting lattice distortion permits weight-percent U concentrations, in agreement with the natural occurrence of elbrusite ($Ca_3(Zr_{1.5}\ U^{6+}_{0.5})\ Fe^{3+}_3\ O_{12}$), a ferrite garnet in which U is a major element (Galuskina et al., 2010; Rak et al., 2011). One possible mechanism for U incorporation is the type of co-substitution found in elbrusite of U^{6+} with a 2+ species at the *Y*- and *Z*-sites of schorlomite group garnet; schorlomite itself ($Ca_3Ti_2(SiO_4)(Fe^{3+}O_4)_2$) forms a solid solution with the silicate garnet group (Grew et al., 2013). This hypothesized mechanism makes the useful prediction that U should co-occur with Ti and/or Zr, and Fe^{3+} in garnet group minerals, although these need only occur in trace quantities as only trace quantities of U are required for U-Pb analysis. However, as Pb may directly substitute for Fe^{2+}, Mn, Ca, and Mg in the garnet group *X*-site (subject to ionic radius constraints; Grew et al., 2013), it follows that initial U/Pb ratios during crystallization may be undesirably low unless Pb has been sequestered in another phase (e.g., K-feldspar), or bulk rock U/Pb ratios are high (e.g., garnet crystallizing in mantle rocks). Additionally, as with any U-host, garnet is also amenable to fission track and (U-Th-Sm)/He dating, although these lower-temperature thermochronometers have seen limited use (Aciego et al., 2003; Haack & Potts, 1972).

The first garnet U-Pb studies were obliged to employ low-throughput bulk solution analyses, which also rendered screening for U-hosting inclusions challenging (e.g., Burton et al., 1995; Mezger et al., 1989). More recent studies following the development of laser ablation inductively coupled plasma mass spectrometry (LA-ICPMS) have pioneered the use of large spots to compensate for typically low U concentrations (Gevedon et al., 2018; Millonig et al., 2020; Salnikova et al., 2018, 2019; Seman et al., 2017; Yang et al., 2018). Together with the identification of matrix-matched reference materials, this approach has enabled in situ garnet U-Pb analysis. In situ Lu-Hf analysis, previously hampered by insurmountable isobaric interferences of ^{176}Lu and ^{176}Yb on ^{176}Hf, has been enabled by use of an online mass-filtered reaction cell, (LA-ICPMS/MS) which mass-shifts ^{176}Hf by reaction

with ammonia to form an interference-free higher-mass polyatomic ion (Simpson et al., 2021; Woods, 2016). In situ analysis enables the high analytical throughput necessary for routine detrital provenance analysis; if a quadrupole instrument capable of rapid peak jumps is employed, co-monitoring of relevant elemental masses (e.g., Zr, Ti, P, LREE) during analysis also enables efficient screening for U- or Lu-hosting inclusions.

Here, we present results from U-Pb and Lu-Hf double-dating, acquired by LA-Q-ICPMS(/MS) for detrital garnet recovered from the Oligo-Miocene pro-foreland basin of the European Alps, as well as modern Alpine river bedload. The Alps make an ideal test case, as the bedrock geology is well documented, and detrital garnet previously characterized for composition are available (Stutenbecker et al., 2017, 2019). The purpose of this study is to compare detrital garnet with the rutile and zircon U-Pb detrital geochronometers, and to assess whether detrital garnet geochronology preferentially records source area metamorphism, which is difficult to detect using zircon.

1.3. Geological Background of the Study Area

A detailed review of the geological evolution of the Alps is beyond the scope of this study and the following section is intended only as a brief synopsis. Readers are directed elsewhere for in-depth discussion (e.g., Handy et al., 2010, 2015; Schmid et al., 2008; Stampfli & Hochard, 2009). Following the prolonged Variscan orogenic cycle (c. 480–290 Ma; Matte, 2001), development of Neotethyan oceanic basins (including the Piedmont-Liguria and Meliata oceans) led to the separation of Africa from Europe during Late Triassic to Jurassic time, producing an intervening assemblage of continental microplates and ocean basins. Reconstructions of this complex tectonic mosaic remain subject to debate, but recent studies show consensus that the Adria microplate was the southernmost microplate, remained kinematically linked to Africa, and was separated from the adjacent microcontinent to the north, termed Alcapia, by a shear zone rather than an ocean basin (Handy et al., 2010, 2015).

Shortening of the Adria-Europe tectonic system led to the mid-Cretaceous Eoalpine event (c. 140–85 Ma; Handy et al., 2010), comprising partial intra-continental subduction of Alcapia beneath Adria, followed by accretion. Post-Eoalpine, shortening of the Adria-Europe system was accommodated by subduction of the Piedmont-Ligurian ocean north of Adria (Handy et al., 2010), culminating in the Alpine orogen (c. 48–15 Ma). The Eoalpine is restricted to the Austroalpine units, with the exception of the autochthonous Sesia-Dent Blanche units of the western Alps. The central and western Alps are characterized by broadly orogen-parallel metamorphic zones, and include twin parallel chains (internal and external) of crystalline basement massifs (Figure 1). The External Massifs comprise polymetamorphic gneisses which attained amphibolite-granulite facies during the Eo-Variscan and Variscan orogens (c. 480-290 Ma; Matte, 2001) followed by Permo-Triassic magmatism and metamorphism (c. 290–245) (Schuster & Stüwe, 2008), but experienced only moderate (sub-greenschist to greenschist-facies) Alpine metamorphism (Bousquet, Oberhänsli, et al., 2012). The Internal Massifs experienced eclogite- to amphibolite-facies grade metamorphism during the Alpine. Alpine-age HP metamorphism up to eclogite-facies grade occurred between c. 37–30 Ma in the Internal Massifs; and at c. 48–42 Ma in the surrounding Penninic metasedimentary and meta-ophiolitic units (Beltrando et al., 2010; Liati et al., 2009). The Lepontine Dome subsequently experienced an amphibolite-facies Barrovian overprint from c. 32–27 Ma, which was terminated by rapid exhumation between c. 22–15 Ma (Boston et al., 2017; Janots et al., 2009).

2. Materials and Methods

2.1. Sampling Strategy

Here, we report data for samples collected from the bedload of modern rivers draining small, quasi-monolithologic catchments, as well as from the Oligo-Miocene pro-foreland molasse basin. These samples were originally collected by Stutenbecker et al. (2017, 2019), who reported major element chemistry acquired using energy-dispersive X-ray spectrometry and electron microprobe analysis (Figure 2). Sample locations are indicated in Figure 1 and reported in Table 1. The 63–250 μm size fraction was targeted for garnet separation.

2.2. Garnet U-Pb and Trace-Element Analysis by LA-Q-ICPMS

Analyses were conducted at the National Centre for Isotope Geochemistry (NCIG) at University College Dublin using a Teledyne Cetac Analyte G2 ArF 193 nm excimer nanosecond laser ablation system equipped with a HelEx II two-volume cell, coupled to a ThermoScientific iCAP Qc quadrupole ICPMS. Masses monitored comprised

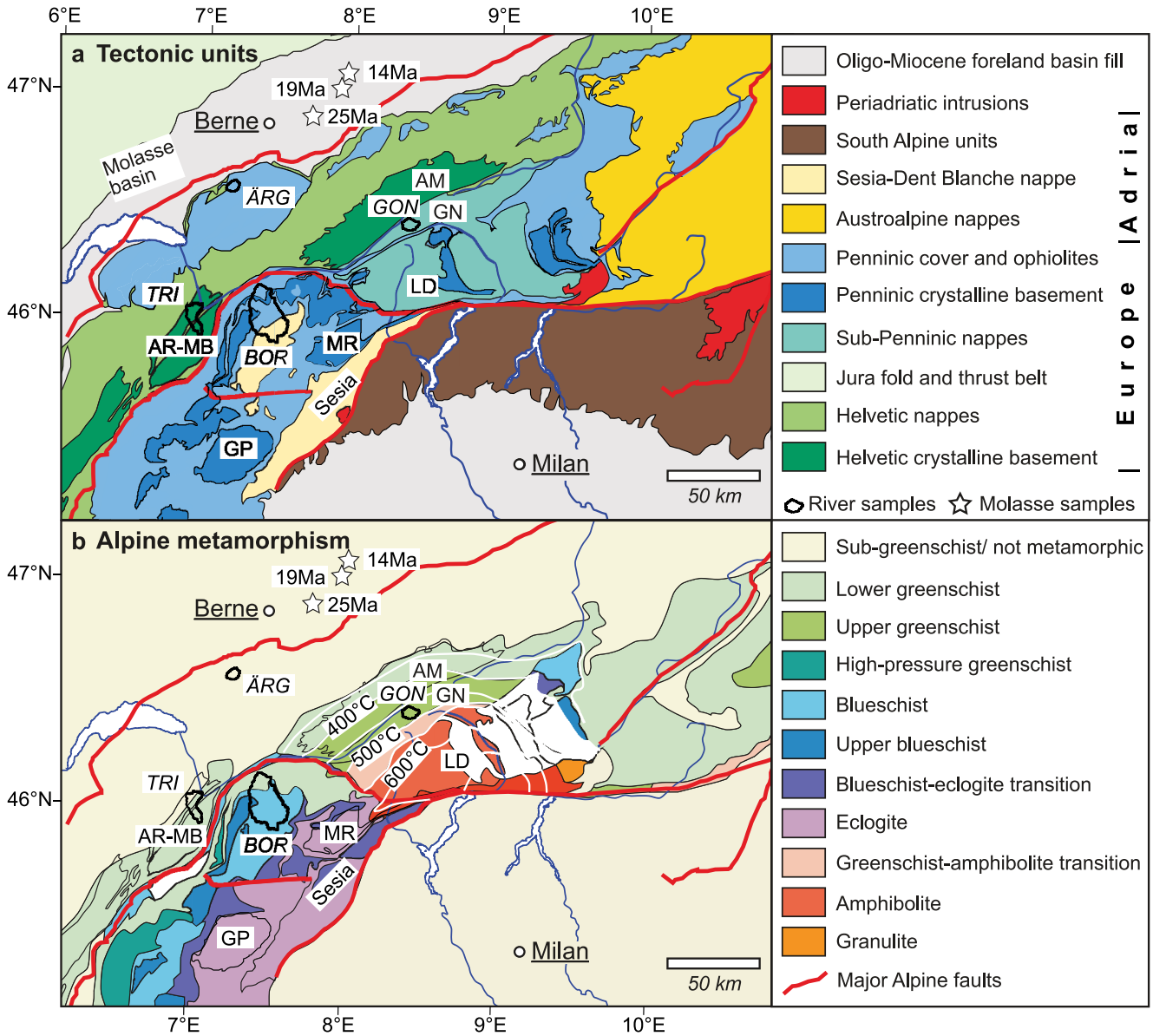

Figure 1. Location map showing (a) tectonic affiliation and (b) metamorphic grade attained during the Alpine orogen, after Bousquet, Oberhänsli, et al. (2012) and Bousquet, Schmid, et al. (2012). AM, Aar Massif; AR-MB, Aiguilles Rouges, Mont Blanc; GN, Gotthard nappe; GP, Gran Paradiso; LD, Lepontine Dome; MR, Monte Rosa. Modern catchments (italicized): TRI, Trient; BOR, Borgne; ÄRG, Ärgera; and GON, Goneri. White stars indicate molasse sampling sites, with deposition ages.

^{25}Mg, ^{27}Al, ^{29}Si, ^{31}P, ^{43}Ca, ^{49}Ti, ^{53}Cr, ^{55}Mn, ^{57}Fe, ^{60}Ni, ^{89}Y, ^{91}Zr, ^{139}La, ^{140}Ce, ^{141}Pr, ^{146}Nd, ^{147}Sm, ^{153}Eu, ^{157}Gd, ^{159}Tb, ^{163}Dy, ^{165}Ho, ^{166}Er, ^{169}Tm, ^{172}Yb, ^{175}Lu, ^{177}Hf, ^{202}Hg, ^{204}Pb, ^{206}Pb, ^{207}Pb, ^{208}Pb, ^{232}Th, and ^{238}U. A spot size of 75 µm was employed; further analytical parameters are fully reported in Table S1. Spikes of P, Ti, Y, Zr, or LREE masses in the time-resolved data were used to identify and exclude U-hosting inclusions during data reduction (Figure S1 in Supporting Information S1). Conventional sample-standard bracketing was employed, with Odikhincha garnet (Salnikova et al., 2019) used as the primary reference material to correct for intra-session analytical drift, mass bias, and downhole fractionation. Data reduction employed the VisualAge_UComPbine data reduction scheme in Iolite 3 (Chew et al., 2014; Paton et al., 2011). Ages were corrected for common-Pb using the ^{207}Pb method, implemented using the iterative approach of Mark et al. (2016), which employs the terrestrial Pb-isotope evolution model of Stacey & Kramers (1975). Age calculations were performed using Isoplot (Ludwig, 2012). As many analyses were discordant due to the incorporation of common-Pb during crystallization, a discordance filter was not applied. However, many analyses exhibited undesirably high age uncertainty. An uncertainty filter was therefore applied following the approach of Chew et al. (2020), such that:

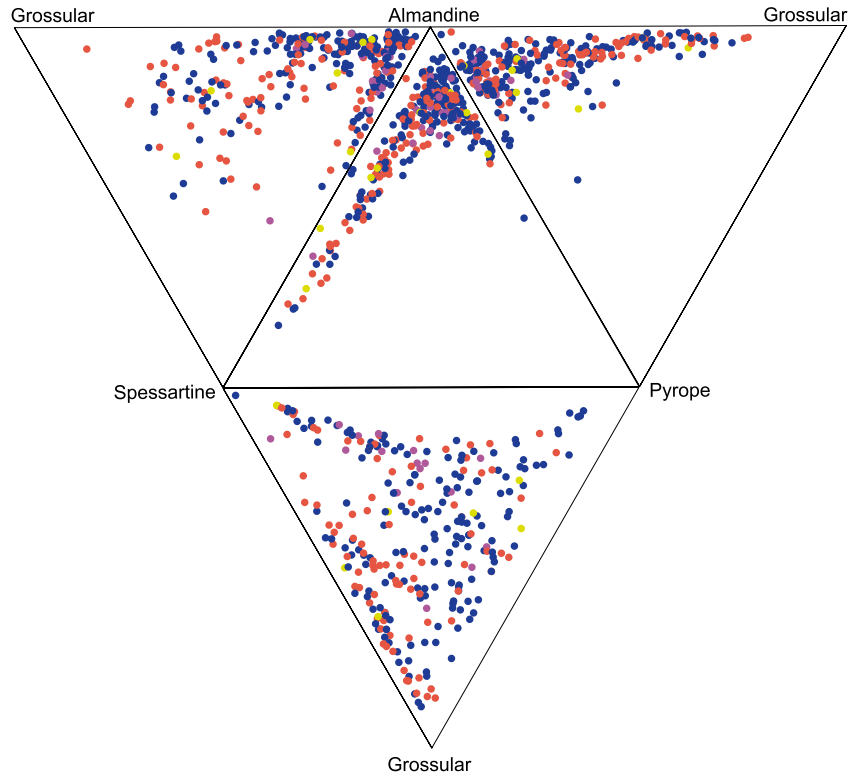

Figure 2. Compositions of garnet analyzed in this study, from Stutenbecker et al. (2017, 2019). Andradite-rich garnets are excluded ($n = 2$). Yellow—double-dated; red—acceptable Lu-Hf age only; purple—acceptable U-Pb age only; blue—no acceptable age recovered.

$$2\sigma(\%)\,\text{limit} = \left(5 \times \text{age}^{-0.5}\right) \times 100$$

Afrikanda, Dashkesan, and Chikskii garnets were used as secondary reference materials and treated as unknowns throughout the data reduction process (reference U-Pb TIMS ages 377 ± 3 Ma, 147 ± 2 Ma, and 492 ± 2 Ma, respectively; Salnikova et al., 2018, 2019; Stifeeva et al., 2019). Afrikanda yielded a lower-intercept U-Pb age of 368.1 ± 2.6 Ma (MSWD = 1.2, $n = 51$), and Dashkesan 146.0 ± 1.3 Ma (MSWD = 0.92, $n = 50$); both are slightly discordant. Chikskii analyses are over-dispersed (MSWD = 3.3) and show signs of both Pb-loss and common-Pb incorporation, so no meaningful age can be reported; this is in agreement with a previous report that the U-Pb system in Chikskii garnet is over-dispersed (O'Sullivan et al., 2023).

Trace element data were also reduced in Iolite using the Trace Elements DRS, employing ^{29}Si as an internal standard to correct for yield variation. The primary reference material was NIST612. As no garnet trace element reference material was available, the komatiite glass GOR-132 was employed as a secondary reference material and treated as an unknown (Jochum et al., 2006). Reference values typically reproduced within 5% despite many being present at ng/g concentrations; an exception was Fe, which was likely affected by a polyatomic Ca-based interference (e.g., Malinovsky et al., 2003). This was aggravated by the unnaturally high reference Ca/Fe ratio in the synthetic NIST glass. U-Pb and trace-element data are fully reported in Table S2.

2.3. Garnet Lu-Hf and Trace-Element Analysis by LA-Q-ICPMS/MS

A subset of 172 grains where sufficient material remained after U-Pb ablation was selected for Lu-Hf analysis. Analyses were conducted at Adelaide Microscopy, The University of Adelaide, using a RESOlution 193 nm laser ablation system (Applied Spectra) with a S155 sample chamber (Laurin Technic), coupled to an Agilent 8900x tandem mass spectrometer (ICPMS/MS). The method involves the addition of NH_3 (supplied as a 1:9 NH_3:He mix for safety reasons) into the reaction cell of the mass spectrometer (at a rate of 3 mL min^{-1}) to promote efficient formation of the $Hf((NH)(NH_2)(NH_3)_3)^+$ reaction product as a direct proxy for ^{176}Hf. Equivalent reaction products for isobars ^{176}Lu and ^{176}Yb are negligible, allowing ^{176}Hf and ^{176}Lu to be effectively separated and

Table 1
Samples Used in This Study, Collected by Stutenbecker et al. (2017, 2019)

Sample	Type	Lat	Long	Description	Deposition age (Ma)	nL/nU/nC	Principal units in catchment
LS2017-3	Molasse bedrock	47.0057	7.9713	UFM—Napf	14	15/0/47	–
LS2018-5	Molasse bedrock	46.9391	7.9508	UMM—Luzern	19	0/2/41	–
LS2016-18	Molasse bedrock	46.7746	7.7324	LFM—Thun	25	8/10/51	–
LS2018-12	MRS	46.7203	7.2455	Ärgera R.	–	5/1/32	Gurnigel flysch
LS2014-19	MRS	46.2242	7.4072	Borgne R.	–	7/1/20	St Bernard-Combin-Dent Blanche nappes
LS2014-29	MRS	46.5330	8.3574	Goneri R.	–	56/2/85	Gotthard nappe
LS2014-37	MRS	46.1323	7.0463	Trient R.	–	9/3/41	Mont Blanc—Aiguilles Rouges external massif

Note. MRS, modern river sediment; UFM, upper fluvial molasse; UMM, upper marine molasse; LFM, lower fluvial molasse; nL, number of acceptable Lu-Hf ages; nU, number of acceptable U-Pb ages; nC, number of garnet compositions. Deposition ages from magnetostratigraphy of Schlunegger et al. (1996).

measured free from isobaric interferences (Glorie, Hand, et al., 2023; Simpson et al., 2021, 2022). Following Simpson et al. (2021), $^{176+82}$Hf was measured as a proxy for ^{176}Hf; ^{175}Lu was measured as a proxy for ^{176}Lu, and $^{178+82}$Hf was measured as a proxy for ^{177}Hf. Isotope ratios were calculated in LADR (Danyushevsky & Norris, 2018) using NIST 610 as a primary standard (Nebel et al., 2009), and corrected for matrix-induced fractionation using Hogsbo garnet (1,029 ± 1.7 Ma; Romer & Smeds, 1996; Simpson et al., 2021). Analytical parameters are fully reported in Table S1. Lu-Hf and trace-element data are fully reported in Table S2.

Resulting Lu-Hf dates were calculated as 2-point (inverse) isochron ages in IsoplotR (Vermeesch, 2018), where the second point comprised an initial ^{177}Hf/^{176}Hf anchor of 3.55 ± 0.05, which spans the entire range of initial ^{177}Hf/^{176}Hf ratios of the terrestrial reservoir (e.g., Glorie, Hand, et al., 2023; Spencer et al., 2020). The obtained inverse isochron age for secondary reference material BP-1 garnet was 1,752 ± 21 Ma (2σ uncertainty including propagated uncertainty from Hogsbo), which is in good agreement with previously published Lu-Hf dates (1,745 ± 14 Ma and 1,744 ± 13 Ma; Glorie, Mulder, et al., 2023; Simpson et al., 2023, respectively). The same uncertainty filter applied to the U-Pb ages was employed.

2.4. Garnet OH and Luminescence Analysis by Raman Spectroscopy

A subset of garnets (n = 45), including those grains yielding acceptable U-Pb or Lu-Hf ages where sufficient material remained after ablation, was selected for Raman spectroscopic analysis. The objective was to assess whether some combination of the Si-O stretching modes represented by "peak 6" (the main high-frequency band in the 870–927 cm^{-1} range of Bersani et al. (2009)), OH stretching signals of the OH groups, and laser-induced luminescence bands could be used to rapidly and non-destructively identify grains amenable to dating.

Raman spectra of garnet grains were collected at the Laboratory for Provenance Studies (University of Milano-Bicocca, Italy) using a Renishaw inVia confocal Raman spectroscope, equipped with a Leica DM2500 microscope. Non-polarized micro-Raman spectra were obtained in nearly backscattered geometry, with a green 532 nm line, solid-state laser, with a spectral resolution of ±0.5 cm^{-1}, and power ≤10 mW at the sample. Before each experimental session, the system was calibrated using a silicon wafer, having its Raman peak at 520.6 ± 0.3 cm^{-1}. A 50x LWD (long working distance) objective or, when applicable, a 20x objective was used. The acquisition of each spectrum was set at 1 s of exposure, 100% of laser power and 30 accumulations. First, the analytical region was centered at 1,090 cm^{-1} (corresponding to a 146–1,912 cm^{-1} spectrum range) in order to detect the six characteristic Raman peaks of garnets, following Bersani et al. (2009). The spectra were elaborated using a Renishaw Windows®-based Raman Environment (WiRE, v. 4.4) software for determining the Raman frequencies of the peaks. Second, the analytical region was centered at 3,700 cm^{-1}, to observe any Raman bands related to the occurrence of OH groups. Raman luminescence fingerprint was also analyzed in the high frequency region centered at 4,300 cm^{-1}. Raman spectroscopic data are fully reported in Table S3.

3. Results

Age spectra for all analyzed garnets are shown in Figure 3; interactive Figure S2 shows the relationship between garnet composition and age recovery. The Lu-Hf data yield a major modal age peak at c. 25 Ma, plus a subordinate peak at c. 330 Ma; the U-Pb data yield corresponding peaks at c. 28 Ma and c. 332 Ma, plus a peak at c. 434 Ma. 28 acceptable U-Pb and 109 acceptable Lu-Hf ages were obtained, representing success rates of 8% and 63% respectively. Nine grains yielded acceptable ages for both systems. Raman data showed no correlation with whether an acceptable U-Pb or Lu-Hf age could be recovered, so are not discussed further.

4. Discussion

Garnet U-Pb age recovery is poor, likely due to low initial U/Pb during crystallization. As shown in Figure 4, garnet in this study is not significantly enriched in U relative to Pb during crystallization, unlike other common-Pb hosting geochronometers (e.g., rutile and apatite). Ideally the U-hosting phase effectively excludes common-Pb during crystallization (e.g., zircon), but at least some degree

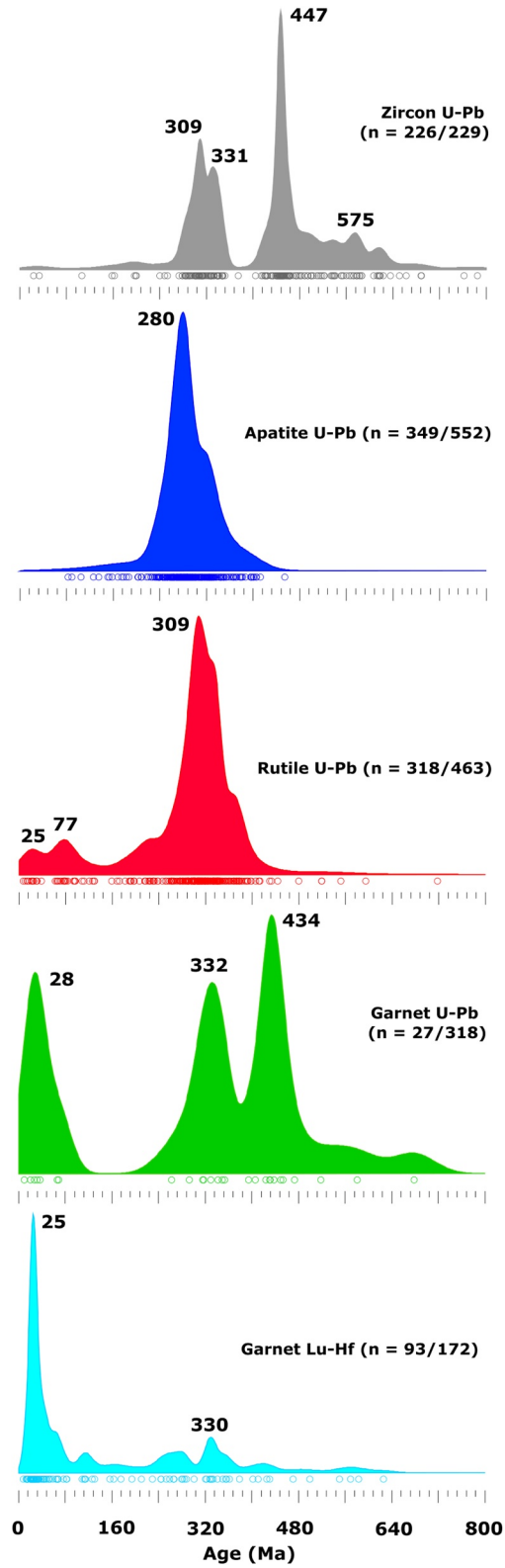

Figure 3.

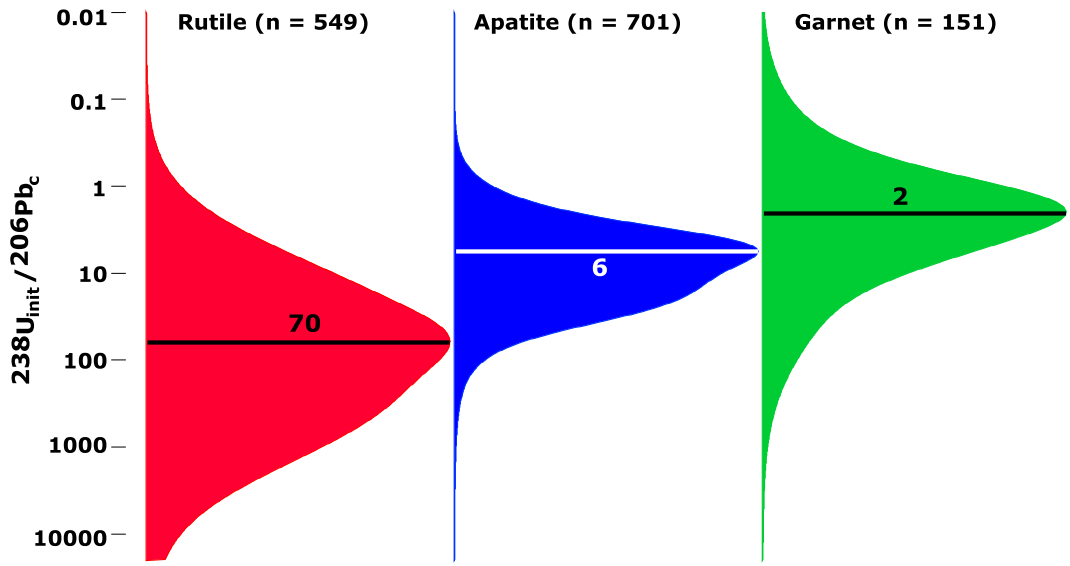

Figure 4. Distribution and modal values of initial $^{238}U/^{206}Pb_c$ ratios at the time of crystallization, calculated for Alpine rutile, apatite, and garnet. Rutile and apatite data are from Mark et al. (2018). Garnet data are from this study. Plots include all analyses for which a finite age could be calculated, regardless of uncertainty.

of U enrichment is required to permit sufficient ingrowth of radiogenic Pb over geologically relevant timescales. Lu-Hf age recovery is considerably better, but still hampered by relatively low Lu concentrations and the relative youthfulness of the Alpine orogen which reduces the time for ingrowth of ^{176}Hf. There is no systematic relationship between garnet composition and whether or not an acceptable age could be obtained (Figure 5a). Trace element data show a weak correlation between age recovery and both decreasing Eu and increasing Y + HREE content (Figure 5b); however, as all age categories overlap, the relationship is not significant.

We also applied the classifier of Schönig et al. (2021) to the EDS-SEM data for these grains reported by Stutenbecker et al. (2017, 2019). This assigns a likeliest source lithology metamorphic facies grade to detrital garnet using a random forest comparison to a bedrock garnet database, as well as classifying non-metamorphic garnet as either igneous, metasomatic, or mantle in origin (the latter category not observed in our data set). This facies classification shows a clearer relationship than the trace-element and compositional data (Figure 6): metamorphic garnet is slightly more likely to be undateable than igneous or metasomatic garnet, suggesting a possible lithological bias for both radioisotope systems.

However, most of the garnets analyzed here are almandine-rich (70% are majority-almandine and 80% are plurality-almandine). While this may approximate the average garnet composition in the continental crust, we cannot exclude the possibility that garnet end members from lithologies which are volumetrically less common at the Earth's surface may exhibit a systemic relationship between composition and amenability to dating. For example, pyrope-rich mantle garnet may be more amenable to U-Pb dating as bulk Pb is extremely low in such rocks (e.g., O'Sullivan et al., 2023). Garnet U content is known to correlate with composition (Deng et al., 2022), but it is the initial U/Pb_c ratio which determines whether an acceptable age can be obtained. In addition, a detailed investigation of potential relationships between source lithology and amenability to dating requires a bedrock rather than a detrital data set.

4.1. Interpretation of Detrital Garnet Ages

The observed garnet U-Pb and Lu-Hf age peaks fit well with known hinterland tectonometamorphic events. The c. 25–28 Ma age peak records the Barrovian overprint in the Lepontine Dome (Boston et al., 2017; Janots

Figure 3. Kernel density estimates for zircon, apatite, rutile, and garnet U-Pb ages, and garnet Lu-Hf ages. Zircon data are from Honegg-Napf molasse samples of Zimmermann et al. (2018), corresponding to Thun-Napf samples of this study; apatite and rutile data are from Honegg-Napf molasse samples of Mark et al. (2018); and garnet data are from this study. Density plots generated using DensityPlotter (Vermeesch, 2012). Data are filtered after the approach of Chew et al. (2020), except for zircon, which is filtered using a concordance probability threshold as described by Zimmermann et al. (2018); n = number of acceptable ages/total analyses. A small number of ages >800 Ma are excluded for clarity (17 zircon; 1 apatite; 0 rutile; 1 garnet U-Pb; and 1 garnet Lu-Hf).

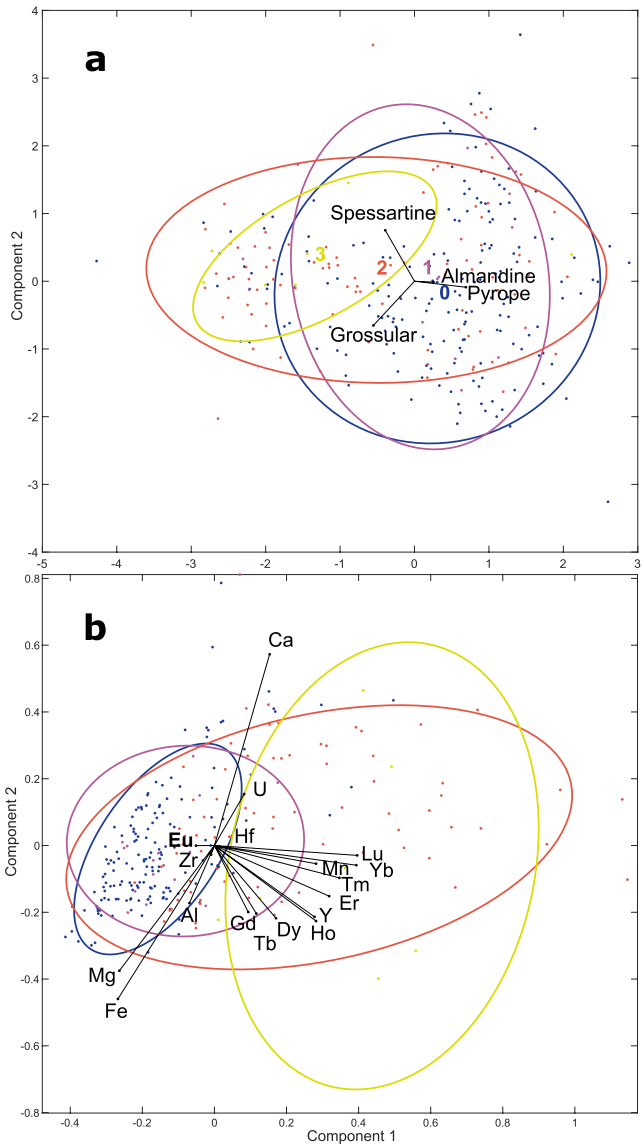

Figure 5. Principal component analysis plots illustrating the lack of correlation between garnet composition and age recovery (blue—no age obtained; purple—U-Pb age only; red—Lu-Hf age only; yellow—age from both systems) for (a) garnet type and (b) major and trace elements. Major element data are from SEM-EDS; trace-element data from laser ablation inductively coupled plasma mass spectrometry. Ellipses are 1 standard deviation.

et al., 2009; Liati et al., 2009). The c. 330–332 Ma age peak records Variscan metamorphism during the collision of Laurussia and Gondwana, which is widely preserved in polycyclic Alpine crystalline bedrock (e.g., von Raumer et al., 2009). The c. 434 Ma U-Pb peak records a Siluro-Ordovician metamorphic event documented in polycyclic units of the external massifs (Schulz & von Raumer, 2011), probably caused by docking of Armorica and Gondwana (Matte, 2001). Preservation of pre-Alpine detrital garnet in sedimentary units incorporated into the Alpine orogen and subjected to blueschist facies metamorphism has also been documented (Manzotti & Ballèvre, 2013).

Using the classifier of Schönig et al. (2021), garnet deposited c. 25 Ma in the pro-foreland (Lower Fluvial Molasse) is dominantly from amphibolite-facies-grade sources, in contrast to garnet deposited at c. 19 and 14 Ma (Upper Marine Molasse and Upper Fluvial Molasse, respectively; Figure 7). Garnet from modern bedload of the Trient and Ärgera rivers, which drain catchments which experienced either no or low-grade Alpine metamorphism (where low-grade is defined as lower- or sub-greenschist-facies-grade), also contains a high proportion of amphibolite-facies-grade grains (Figures 1b and 7). Widespread Alpine amphibolite-facies-grade metamorphism is restricted to the Lepontine Dome and dates to c. 32–27 Ma, followed by rapid exhumation between c. 22 and 15 Ma (Boston et al., 2017; Janots et al., 2009).

Therefore, the Lepontine Dome is unlikely to be the source of the amphibolite grade garnet deposited at c. 25 Ma. Instead, these observations are consistent with garnet deposited at c. 25 Ma being dominantly sourced from pre-Alpine metamorphic bedrock, either directly or recycled via pre-Miocene sedimentary rocks. The decrease in amphibolite grade garnet and increase in garnet from other metamorphic grades during c. 19–14 Ma is consistent with increasing input from units which experienced Alpine metamorphism, for example, the upper greenschist-grade parts of the Aar-Gotthard massif drained by the modern Goneri catchment, and perhaps the now-eroded greenschist-grade upper levels of the Lepontine Dome. Thus, our data are consistent with exposure of the Gotthard nappe and partial unroofing of the Lepontine Dome during 19–14 Ma, in agreement with the conclusions of Stutenbecker et al. (2019).

Our data set of garnet ages is too small to be reliably interpreted by sample: we report only 128 grains with acceptable ages, compared to 291 compositions. Therefore, many samples yield very small numbers of dated grains (Table 1). However, we note that all the garnets yielding acceptable ages ($n = 19$) deposited at 25 Ma yield ages >280 Ma, that is, pre-Alpine (including 7 amphibolite grade garnets). All but two of the garnets deposited at 19–14 Ma yield ages <110 Ma, that is, Alpine ($n = 17$). While this observation is consistent with the source facies classifications, we caution that the sample sizes are too small to be considered robust.

However, the garnet U-Pb and Lu-Hf age spectra clearly differ, with the U-Pb system preserving more pre-Alpine ages. It is also important to consider that most garnets analyzed here did not yield acceptable ages for both systems; therefore, some of the garnets yielding Carboniferous and Silurian U-Pb ages could be from sources which were not strongly affected by the Alpine orogen or which were otherwise shielded, and might have yielded compatible Lu-Hf ages had sufficient Lu been present. Nonetheless, as previously observed for other phases (e.g., the U-Pb and Lu-Hf systems in apatite; Glorie et al., 2022), garnet ages obtained from the same sample using multiple dating methods need not always agree within analytical uncertainty (e.g., Smit et al., 2013). Such disagreement is expected where radioisotope systems hosted in the same phase have differing diffusivities.

Other causes of over-dispersion may include inclusions and parent zonation during geologically prolonged or polyphase mineral growth. Note that these mechanisms are not mutually exclusive. Where in situ analysis

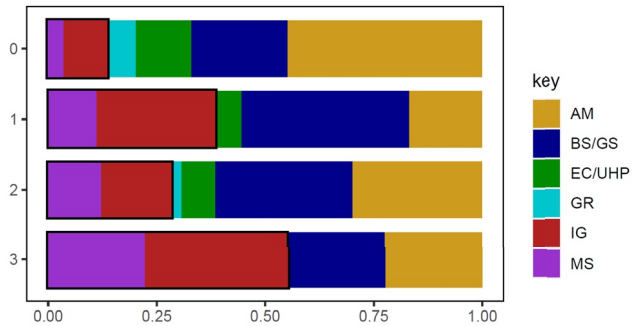

Figure 6. Garnet (modern bedload and pro-foreland molasse) classified using the scheme of Schönig et al. (2021), grouped by age recovery: 0—no age obtained; 1—acceptable U-Pb age obtained; 2—acceptable Lu-Hf age obtained; 3—both systems yielded acceptable ages. AM, amphibolite facies grade; BS/GS, blueschist/greenschist facies grade; EC/UHP, eclogite/ultrahigh-pressure facies grade; GR, granulite facies grade; IG, igneous rocks; MS, metasomatic rocks.

is employed, as here, inclusions are readily detected and excluded by co-analysis of elements stoichiometric to the included phases. Parent isotope zonation effects may be induced either by Raleigh fractionation (Kohn, 2009) or by polyphase growth, and could cause different radioisotope systems to record different geological events if the parent isotope concentrations are anticorrelated, for example, Lu enrichment in the core and U in the rim (e.g., Raimondo et al., 2017). However, in detrital studies, the small age offsets caused by such fractionation effects may be negligible where the objective is to distinguish between geological events which are well separated in time, such as different orogens.

Finally, polyphase growth recording multiple orogenic events is likely to be less important in garnet than in more refractory geochronometers (e.g., the U-Pb system in zircon) because relict or detrital garnet is thought to seldom survive diagenesis and the early stages of prograde metamorphism (Cave et al., 2015; Garzanti et al., 2018; Manzotti & Ballèvre, 2013). However, inherited garnet, which is retained in polycyclic crystalline bedrock without being released to the sedimentary system, may record multiple metamorphic events (e.g., Argles et al., 1999; Simpson et al., 2023; Walker et al., 2021). Polyphase garnet is thus a possible mechanism for the differing U-Pb and Lu-Hf ages, although it is not clear why this would preferentially cause one radioisotope system to record older ages unless U was preferentially incorporated during core growth.

To assess whether the different U-Pb and Lu-Hf age spectra could arise from diffusivity differences, we calculate the closure temperatures for both systems (Dodson, 1973) in Matlab®. The diffusivity of Lu and Hf has recently been experimentally re-evaluated in gem-quality natural spessartine garnet (Bloch et al., 2015, 2020). Unusually, both parent and daughter elements are proposed to diffuse at geologically reasonable cooling rates and grain sizes. While the closure temperature for Hf in garnet is typically >730°C, Lu may be mobile at temperatures as low as 600–700°C for grain radii <100 μm, provided cooling rates are below c. 1°C/Ma (Figures 8a and 8b). However, at the low concentrations typical in natural garnet, significant Lu diffusion was observed in experiments at atmospheric pressure but not where experimental pressures exceeded 1 GPa (Bloch et al., 2020). As experiments at intervening pressures were not performed by Bloch et al. (2020), it is unclear whether significant Lu diffusion may be expected at geologically typical PT conditions. The documented preservation of oscillatory Lu zoning in garnet growing during prograde conditions >600°C and <1 GPa suggests that Lu diffusion in geologically relevant PT conditions may be less significant than experimental data suggest (Guilmette et al., 2018). A pressure

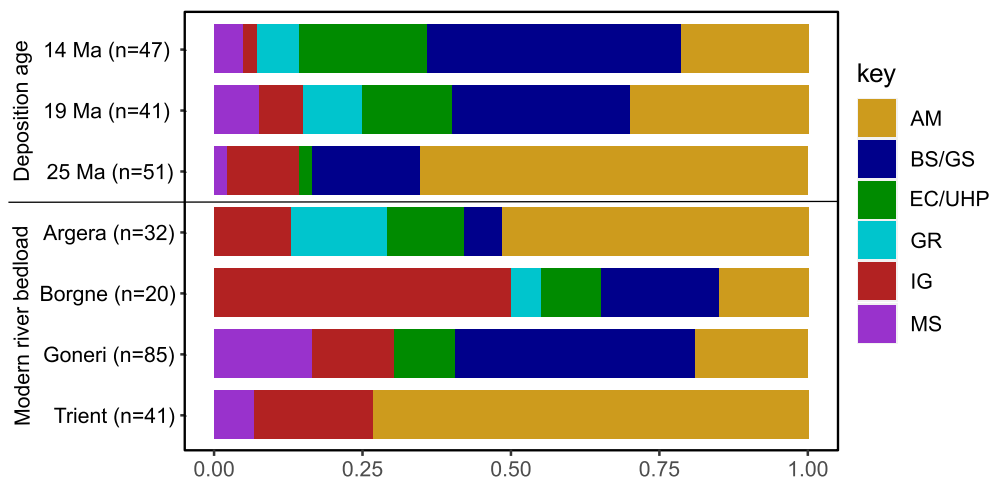

Figure 7. Pro-foreland molasse and modern river bedload garnet classification by metamorphic facies grade (plus igneous and metasomatic fractions), using the classifier of Schönig et al. (2021). UFM, upper fluvial molasse; UMM, upper marine molasse; LFM, lower fluvial molasse. AM, amphibolite facies grade; BS/GS, blueschist/greenschist facies grade; EC/UHP, eclogite/ultrahigh-pressure facies grade; GR, granulite facies grade; IG, igneous rocks; MS, metasomatic rocks.

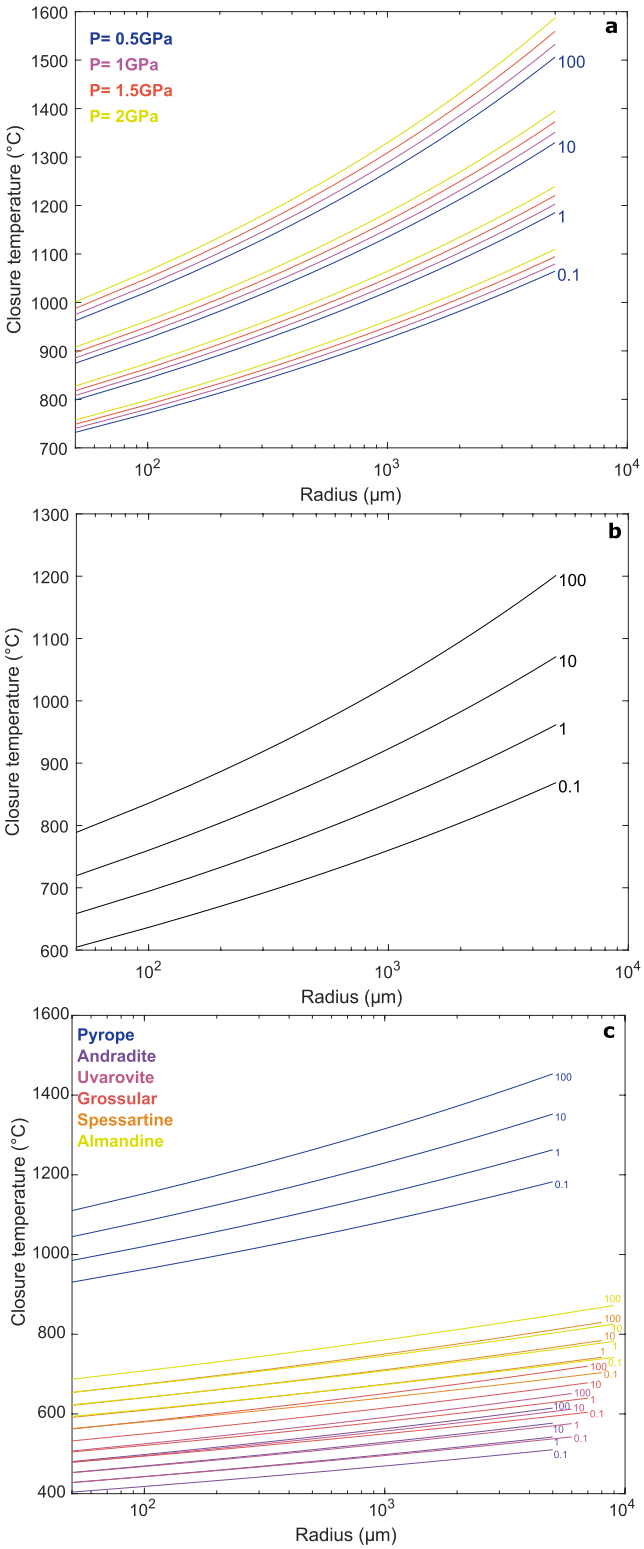

Figure 8. Closure temperature estimates for (a) Hf, (b) Lu, and (c) Pb in garnet, for cooling rates of 0.1–100°C Ma^{-1}.

control was more definitively documented for Hf diffusivity, but the effect is relatively minor: a 1.5 GPa increase in pressure increases closure temperature by <8% (Bloch et al., 2020). A dependence on Si activity is even more minor and is not considered here.

For the U-Pb system in garnet, experimental diffusivity data are unfortunately not available and empirical data are limited. Therefore, we use Pb diffusivity documented in other phases and the empirical relationship between ionic porosity and diffusivity to estimate closure temperatures (Dahl, 1997; Zhao & Zheng, 2007). The resulting estimates show a strong compositional control, with the U-Pb system in pyrope having very high closure temperatures (Figure 8c). As the closure estimates presented here are for pure end-members, it is not clear how to quantify closure temperature for more commonly observed intermediate garnet compositions. However, the majority of garnets analyzed in the study are almandine-dominated, which is the second most retentive end-member for Pb after pyrope. Thus, garnets dominated by almandine-pyrope conceivably have higher closure temperatures for U-Pb than for Lu-Hf, especially at low pressures where Lu may be mobile. Unfortunately, it is not possible to calculate Lu-Hf closure temperatures in other garnet end-members for direct comparison using the ionic porosity model, as Hf diffusivity has been determined only in a small number of phases, some of which exhibit very similar diffusivity (almandine, forsterite, rutile, spessartine, and zircon; Bloch et al., 2015, 2020; Cherniak, 2003; Cherniak et al., 2007; Jollands et al., 2014). However, measured diffusivities for these minerals do not display a linear relationship to ionic porosity identified by Zhao and Zheng (2007), and REE and Hf diffusivity was not observed to vary significantly between almandine and spessartine garnet (Bloch et al., 2015).

However, for the small subset ($n = 9$) of garnets analyzed here, which yielded both acceptable Lu-Hf and U-Pb ages, the ages from both systems define a line with a slope and intercept within the uncertainty of one and zero, respectively, when plotted together (Figure 9). The small sample size means that the relationship should be treated with some caution, and some ages are clearly in disagreement. Nonetheless, these double-dated grains suggest that ages obtained from both systems are likely to be in agreement, and do not indicate a systematic tendency for either radioisotope system to yield older ages, which would be expected if one system had significant diffusivity at Alpine metamorphic temperatures.

4.2. Relationship of Detrital Garnet Ages to Other Detrital Geochronometers

The detrital garnet Lu-Hf and U-Pb ages can also usefully be compared with the age spectra of other detrital geochronometers recovered from the same molasse units (Figure 3). The Alpine orogen is essentially unrecorded by the U-Pb system in zircon, due to the very limited degree of anatexis, which is restricted to the Periadriatic line plutons (e.g., the Bergell and Adamello). Outwith these volumetrically small intrusions, Alpine zircon neocrystallization is limited to epitaxial overgrowth (Rubatto & Hermann, 2003). The U-Pb system in apatite also yields only a small number of Alpine ages, and is dominated by Variscan metamorphism and post-Variscan magmatism (c. 290 Ma; Cassinis et al., 2011). While Alpine rocks yield abundant apatite, the widespread greenschist to amphibolite facies grade metamorphism of the central Alps is associated with low-U apatite, likely rendering many Alpine-age apatite grains undatable by U-Pb (Henrichs et al., 2019; Malusà

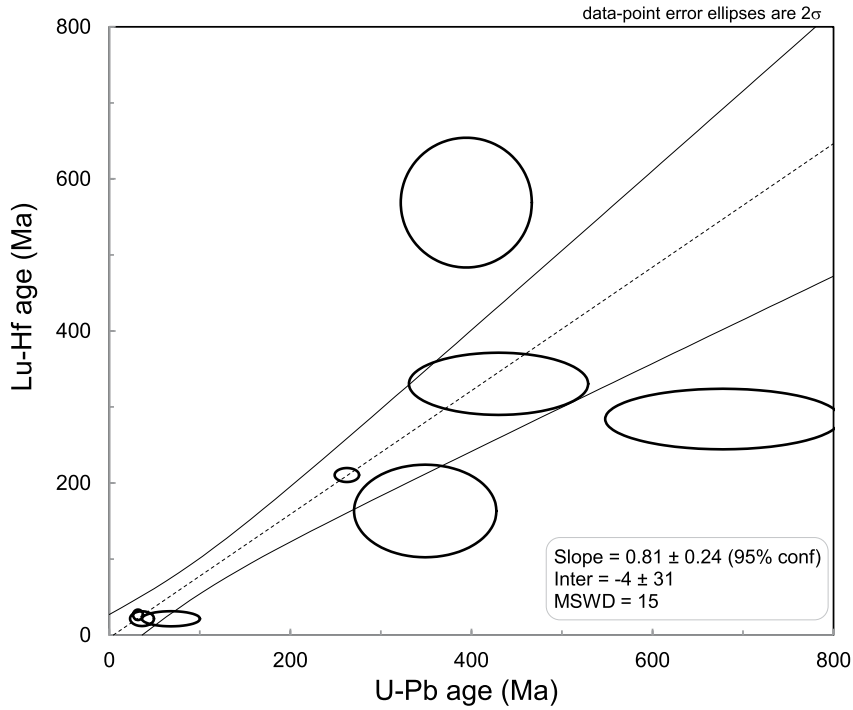

Figure 9. $Age_{U\text{-}Pb}$ versus $Age_{Lu\text{-}Hf}$ for double-dated garnets ($n = 9$) yielding acceptable ages for both systems. These define a line with a slope and intercept within an uncertainty of one and zero, respectively; however, some ages are not in agreement as indicated by the high MSWD. Consistent agreement between the two age systems is not necessarily expected given the differences in closure temperature, and the possibility of dating different age domains within the same grain.

et al., 2017). The U-Pb system in rutile does yield subordinate Alpine age peaks, but at c. 77 Ma and c. 25 Ma; the former likely records Eoalpine metamorphism in the Sesia unit, and the latter likely records cooling through the Pb partial retention zone toward the end of the Lepontine Barrovian overprint. However, the dominant rutile U-Pb age peaks are Variscan.

Thus, detrital garnet ages appear strongly biased toward the most recent garnet-crystallizing metamorphic event, with fewer pre-Alpine ages than other detrital geochronometers. This is probably due to garnet being much less refractory than rutile or zircon, although polycyclic garnet has been documented (e.g., Argles et al., 1999; Manzotti & Ballèvre, 2013). The U-Pb system in detrital rutile also provides a proxy for metamorphism as rutile rarely forms as a primary igneous mineral (Force, 1980), but the much more refractory nature of rutile means that a larger number of polycyclic grains yielding inherited ages are likely to be analyzed as well. Garnet is readily removed from heavy mineral assemblages during diagenesis; in contrast, rutile, together with zircon and tourmaline, is typically among the most persistant heavy minerals (Hubert, 1962). Both garnet and rutile are also likely to break down during the sub- and lower-greenschist-facies-grade stages of prograde metamorphism (Cave et al., 2015; Force, 1980). Detrital garnet geochronology may thus hold potential as a proxy for the most recent mid-grade metamorphism in the source area, especially for less deeply eroded orogens preserving widespread metapelitic rocks which are likely to be rich in garnet.

In this context, mid-grade metamorphic source rocks attain sufficiently high pressures and temperatures to crystallize garnet, but fall short of anatexis and therefore do not crystallize zircon. The PT conditions for the garnet-in isograd will evidently vary considerably depending on rock composition, but temperature estimates between c. 450–550°C for metapelitic rocks are commonly reported, that is, within the upper-greenschist-facies- and upper-blueschist-facies-grades (e.g., Florence & Spear, 1993). However, spessartine-rich garnet is stabilized in Mn-rich metapelites at temperatures at least as low as 400°C (White et al., 2014) and potentially as low as 300–350°C (Kennan & Murphy, 1993), showing the importance of integrating garnet composition with age interpretation. These temperatures are lower than typical rutile formation temperatures of >c. 450°C (Chambers & Kohn, 2012), illustrating that detrital garnet geochronology may be usefully applied to lower-grade orogens which did not extensively crystallize rutile. While such orogens may also be appropriate targets for $^{40}Ar/^{39}Ar$

or $^{87}Rb/^{87}Sr$ analysis of detrital mica, garnet is less prone to alteration or hydrodynamic fractionation during transport (Garzanti et al., 2008).

Additionally, the overlap between Alpine garnet and rutile ages suggests that post-peak cooling to temperatures below the thermal sensitivity of the U-Pb system in rutile must have been geologically rapid, that is, within c. 1–2 Ma. Diffusivity of Pb in rutile is well established, with experimental and empirical studies indicating a partial retention zone of c. 490–640°C for geologically typical grain sizes and cooling rates (Cherniak, 2000; Kooijman et al., 2010). Thermal sensitivity of both the U-Pb and Lu-Hf systems in garnet is less well constrained, but considered to be c. 600–1050°C for the almandine-dominated garnets analyzed here, of typical detrital grain size (50–100 µm radius) subjected to geologically common cooling rates (Bloch et al., 2020; O'Sullivan et al., 2023; Smit et al., 2013). Therefore, prolonged residence at temperatures >490°C would be expected to yield rutile U-Pb ages younger than garnet ages. Similar rutile and garnet Alpine ages agree with documented rapid cooling of the Lepontine Dome and southern Aar-Gotthard massif between c. 22 and 15 Ma (Boston et al., 2017; Janots et al., 2009).

5. Conclusions

Both the U-Pb and Lu-Hf isotope systems in garnet are biased toward the youngest garnet-crystallizing metamorphic event in the source area, in agreement with the less refractory nature of garnet compared to rutile or zircon. Detrital garnet geochronology therefore shows utility where the objective is to identify sediment sourced from the youngest and, hence, likely most rapidly exhumed component of an orogen without co-analysis of large numbers of inherited ages. Age recovery for both systems is not compositionally biased, at least for the generally almandine-rich garnets analyzed here. However, the Lu-Hf system shows considerably better age recovery than the U-Pb system (8% vs. 63%), due to the failure of garnet to concentrate U relative to Pb during crystallization. While possible compositional and pressure controls on both the U-Pb and Lu-Hf system in garnet may complicate age interpretation, the ability of this study to reproduce the age of Alpine Barrovian metamorphism indicates that these complexities are generally unimportant. Detrital garnet Lu-Hf dating, coupled in future with compositional analysis and crystallization pressure estimates using thermoba-Raman-try (Kohn, 2014) and Zr-in-rutile or –titanite detrital thermometry, may offer scope for rapid first-order reconstruction of source area pressure-time evolution, especially in areas difficult to access directly.

Data Availability Statement

The data reported in this study (Mark et al., 2023) are fully tabulated in the supplementary materials accessible at https://doi.org/10.5281/zenodo.7900189. The software packages used for U-Pb and Lu-Hf data reduction were Iolite (a division of Elemental Scientific, Inc.) and LADR (Norris Scientific PTY LTD). Both data reduction packages are available under proprietary license.

Acknowledgments
The authors acknowledge financial support from Science Foundation Ireland (Starting Investigator Research Grant 18/SIRG/5559 to CM), the Australian Research Council (Future Fellowship FT210100906 to SG), and the Irish Research Council (Government of Ireland Postdoctoral Fellowship GOIPD/2019/906 to GO'S). NCIG equipment used in this study was funded by grants from Science Foundation Ireland (13/RC/2092) and the Irish Higher Education Authority through the Programme for Research at Third Level Institutions, Cycle 5 (PRTLI-5). We thank Ekaterina Salnikova for supplying garnet U-Pb reference materials, Matthijs Smit for helpful discussion on Lu-Hf systematics, two anonymous reviewers for constructive comments, and Alberto Resentini and Amy East for editorial handling.

References

Aciego, S., Kennedy, B. M., DePaolo, D. J., Christensen, J. N., & Hutcheon, I. (2003). U-Th/He age of phenocrystic garnet from the 79 AD eruption of Mt. Vesuvius. *Earth and Planetary Science Letters*, *216*(1–2), 209–219. https://doi.org/10.1016/S0012-821X(03)00478-3

Andò, S., Garzanti, E., Padoan, M., & Limonta, M. (2012). Corrosion of heavy minerals during weathering and diagenesis: A catalog for optical analysis. *Sedimentary Geology*, *280*, 165–178. https://doi.org/10.1016/j.sedgeo.2012.03.023

Andò, S., Morton, A., & Garzanti, E. (2013). Metamorphic grade of source rocks revealed by chemical fingerprints of detrital amphibole and garnet. *Geological Society, London, Special Publications*, *386*(1), 351–371. https://doi.org/10.1144/SP386.5

Argles, T. W., Prince, C. I., Foster, G. L., & Vance, D. (1999). New garnets for old? Cautionary tales from young mountain belts. *Earth and Planetary Science Letters*, *172*(3–4), 301–309. https://doi.org/10.1016/s0012-821x(99)00209-5

Baxter, E. F., & Scherer, E. E. (2013). Garnet geochronology: Timekeeper of tectonometamorphic processes. *Elements*, *9*(6), 433–438. https://doi.org/10.2113/gselements.9.6.433

Beltrando, M., Compagnoni, R., & Lombardo, B. (2010). (Ultra-) High-pressure metamorphism and orogenesis: An Alpine perspective. *Gondwana Research*, *18*(1), 147–166. https://doi.org/10.1016/j.gr.2010.01.009

Bersani, D., Andò, S., Vignola, P., Moltifiori, G., Marino, I. G., Lottici, P. P., & Diella, V. (2009). Micro-Raman spectroscopy as a routine tool for garnet analysis. *Spectrochimica Acta - Part A: Molecular and Biomolecular Spectroscopy*, *73*(3), 484–491. https://doi.org/10.1016/j.saa.2008.11.033

Bloch, E., Ganguly, J., Hervig, R., & Cheng, W. (2015). ^{176}Lu–^{176}Hf geochronology of garnet I: Experimental determination of the diffusion kinetics of Lu^{3+} and Hf^{4+} in garnet, closure temperatures and geochronological implications. *Contributions to Mineralogy and Petrology*, *169*(2), 12. https://doi.org/10.1007/s00410-015-1109-8

Bloch, E., Jollands, M. C., Devoir, A., Bouvier, A. S., Ibañez-Mejia, M., & Baumgartner, L. P. (2020). Multispecies diffusion of yttrium, rare earth elements and hafnium in garnet. *Journal of Petrology*, *61*(7). https://doi.org/10.1093/petrology/egaa055

Boehnke, P., Watson, E. B., Trail, D., Harrison, T. M., & Schmitt, A. K. (2013). Zircon saturation re-revisited. *Chemical Geology*, *351*, 324–334. https://doi.org/10.1016/j.chemgeo.2013.05.028

Boston, K. R., Rubatto, D., Hermann, J., Engi, M., & Amelin, Y. (2017). Geochronology of accessory allanite and monazite in the Barrovian metamorphic sequence of the Central Alps, Switzerland. *Lithos*, *286–287*, 502–518. https://doi.org/10.1016/j.lithos.2017.06.025

Bousquet, R., Oberhänsli, R., Schmid, S. M., Berger, A., Wiederkehr, M., Möller, A., et al. (2012). Metamorphic framework of the Alps, *CCGM/CGMW, scale 1:1,000,000*.

Bousquet, R., Schmid, S. M., Zeilinger, G., Oberhänsli, R., Rosenberg, C., Molli, G., et al. (2012). Tectonic framework of the Alps, *CCGM/CGMW, scale 1:1,000,000*.

Burton, K. W., Kohn, M. J., Cohen, A. S., & Keith O'Nions, R. (1995). The relative diffusion of Pb, Nd, Sr and O in garnet. *Earth and Planetary Science Letters*, *133*(1–2), 199–211. https://doi.org/10.1016/0012-821X(95)00067-M

Campbell, I. H., Reiners, P. W., Allen, C. M., Nicolescu, S., & Upadhyay, R. (2005). He–Pb double dating of detrital zircons from the Ganges and Indus Rivers: Implication for quantifying sediment recycling and provenance studies. *Earth and Planetary Science Letters*, *237*(3–4), 402–432. https://doi.org/10.1016/j.epsl.2005.06.043

Cassinis, G., Perotti, C. R., & Ronchi, A. (2011). Permian continental basins in the Southern Alps (Italy) and peri-Mediterranean correlations. *International Journal of Earth Sciences*, *101*(1), 129–157. https://doi.org/10.1007/s00531-011-0642-6

Cave, B., Stepanov, A., Craw, D., Large, R., Halpin, J., & Thompson, J. (2015). Release of trace elements through the sub-greenschist facies breakdown of detrital rutile to metamorphic titanite in the Otago schist, New Zealand. *The Canadian Mineralogist*, *53*(3), 379–400. https://doi.org/10.3749/canmin.1400097

Chambers, J. A., & Kohn, M. J. (2012). Titanium in muscovite, biotite, and hornblende: Modeling, thermometry, and rutile activities of metapelites and amphibolites. *American Mineralogist*, *97*(4), 543–555. https://doi.org/10.2138/am.2012.3890

Cherniak, D. J. (2000). Pb diffusion in rutile. *Contributions to Mineralogy and Petrology*, *139*(2), 198–207. https://doi.org/10.1007/pl00007671

Cherniak, D. J. (2003). Diffusion in zircon. *Reviews in Mineralogy and Geochemistry*, *53*(1), 113–143. https://doi.org/10.2113/0530113

Cherniak, D. J., Manchester, J., & Watson, E. B. (2007). Zr and Hf diffusion in rutile. *Earth and Planetary Science Letters*, *261*(1–2), 267–279. https://doi.org/10.1016/j.epsl.2007.06.027

Chew, D., O'Sullivan, G., Caracciolo, L., Mark, C., & Tyrrell, S. (2020). Sourcing the sand: Accessory mineral fertility, analytical and other biases in detrital U-Pb provenance analysis. *Earth-Science Reviews*, *202*, 103093. https://doi.org/10.1016/j.earscirev.2020.103093

Chew, D., Petrus, J. A., & Kamber, B. S. (2014). U-Pb LA-ICPMS dating using accessory mineral standards with variable common Pb. *Chemical Geology*, *363*, 185–199. https://doi.org/10.1016/j.chemgeo.2013.11.006

Christensen, J. N., Rosenfeld, J. L., & DePaolo, D. J. (1989). Rates of tectonometamorphic processes from rubidium and strontium isotopes in garnet. *Science*, *244*(4911), 1465–1469. https://doi.org/10.1126/science.244.4911.1465

Connally, G. G. (1964). Garnet ratios and provenance in the glacial drift of western New York. *Science*, *144*(3625), 1452–1453. https://doi.org/10.1126/science.144.3625.1452

Dahl, P. S. (1997). A crystal-chemical basis for Pb retention and fission-track annealing systematics in U-bearing minerals, with implications for geochronology. *Earth and Planetary Science Letters*, *150*(3–4), 277–290. https://doi.org/10.1016/s0012-821x(97)00108-8

Danyushevsky, L., & Norris, A. (2018). Software and protocols for improved accuracy of LA-ICP-MS analysis via quantification of matrix effects. Goldschmidt Abstracts 513.

Deng, Y., Zhong, R., Li, D., Li, Y., & Cui, H. (2022). Hunting the datable garnet using the LA-ICP-MS U-Pb method: Predicting garnet U concentration, based on major and minor elements. *Acta Geologica Sinica*, *96*(6), 2148–2157. https://doi.org/10.1111/1755-6724.14921

DePaolo, D. J., & Wasserburg, G. J. (1976). Inferences about magma sources and mantle structure from variations of $^{143}Nd/^{144}Nd$. *Geophysical Research Letters*, *3*(12), 743–746. https://doi.org/10.1029/GL003i012p00743

DeWolf, C. P., Zeissler, C. J., Halliday, A. N., Mezger, K., & Essene, E. J. (1996). The role of inclusions in U-Pb and Sm-Nd garnet geochronology: Stepwise dissolution experiments and trace uranium mapping by fission track analysis. *Geochimica et Cosmochimica Acta*, *60*(1), 121–134. https://doi.org/10.1016/0016-7037(95)00367-3

Dodson, M. H. (1973). Closure temperature in cooling geochronological and petrological systems. *Contributions to Mineralogy and Petrology*, *40*(3), 259–274. https://doi.org/10.1007/BF00373790

do Nascimento, D. R., Sawakuchi, A. O., Guedes, C. C. F., Giannini, P. C. F., Grohmann, C. H., & Ferreira, M. P. (2015). Provenance of sands from the confluence of the Amazon and Madeira rivers based on detrital heavy minerals and luminescence of quartz and feldspar. *Sedimentary Geology*, *316*, 1–12. https://doi.org/10.1016/j.sedgeo.2014.11.002

Duchêne, S., Blichert-Toft, J., Luais, B., Télouk, P., Lardeaux, J. M., & Albarède, F. (1997). The Lu-Hf dating of garnets and the ages of the Alpine high-pressure metamorphism. *Nature*, *387*(6633), 586–589. https://doi.org/10.1038/42446

Florence, F., & Spear, F. (1993). Influences of reaction history and chemical diffusion on P-T calculations for staurolite schists from the Littleton Formation, northwestern New Hampshire. *American Mineralogist*, *78*, 345–359.

Force, E. R. (1980). The provenance of rutile. *Journal of Sedimentary Petrology*, *50*, 485–488.

Galuskina, I. O., Galuskin, E. V., Armbrusteter, T., Lazic, B., Kusz, J., Dzierzanowski, P., et al. (2010). Elbrusite-(Zr)—A new uranian garnet from the Upper Chegem caldera, Kabardino-Balkaria, Northern Caucasus, Russia. *American Mineralogist*, *95*(8–9), 1172–1181. https://doi.org/10.2138/am.2010.3507

Garçon, M., Chauvel, C., France-Lanord, C., Limonta, M., & Garzanti, E. (2014). Which minerals control the Nd–Hf–Sr–Pb isotopic compositions of river sediments? *Chemical Geology*, *364*, 42–55. https://doi.org/10.1016/j.chemgeo.2013.11.018

Garzanti, E., & Andò, S. (2007). Plate tectonics and heavy-mineral suites of modern sands. In M. A. Mange & D. T. Wright (Eds.), *Heavy minerals in use*, *Developments in sedimentology* (Vol. 58, pp. 741–763). Elsevier.

Garzanti, E., Andò, S., France-Lanord, C., Vezzoli, G., Censi, P., Galy, V., & Najman, Y. (2010). Mineralogical and chemical variability of fluvial sediments. 1. Bedload sand (Ganga-Brahmaputra, Bangladesh). *Earth and Planetary Science Letters*, *299*(3–4), 368–381. https://doi.org/10.1016/j.epsl.2010.09.017

Garzanti, E., Andò, S., Limonta, M., Fielding, L., & Najman, Y. (2018). Diagenetic control on mineralogical suites in sand, silt, and mud (Cenozoic Nile Delta): Implications for provenance reconstructions. *Earth-Science Reviews*, *185*, 122–139. https://doi.org/10.1016/j.earscirev.2018.05.010

Garzanti, E., Andò, S., Padoan, M., Vezzoli, G., & El Kammar, A. (2015). The modern Nile sediment system: Processes and products. *Quaternary Science Reviews*, *130*, 9–56. https://doi.org/10.1016/j.quascirev.2015.07.011

Garzanti, E., Andò, S., & Vezzoli, G. (2008). Settling equivalence of detrital minerals and grain-size dependence of sediment composition. *Earth and Planetary Science Letters*, *273*(1–2), 138–151. https://doi.org/10.1016/j.epsl.2008.06.020

Garzanti, E., Pastore, G., Resentini, A., Vezzoli, G., Vermeesch, P., Ncube, L., et al. (2021). The segmented Zambezi sedimentary system from source to sink: 1. Sand petrology and heavy minerals. *Journal of Geology*, *129*(4), 343–369. https://doi.org/10.1086/715792

Garzanti, E., Resentini, A., Vezzoli, G., Andò, S., Malusà, M. G., Padoan, M., & Paparella, P. (2010). Detrital fingerprints of fossil continental-subduction zones (axial belt provenance, European Alps). *The Journal of Geology*, *118*(4), 341–362. https://doi.org/10.1086/652720

Garzanti, E., Vermeesch, P., Vezzoli, G., Andò, S., Botti, E., Limonta, M., et al. (2019). Congo River sand and the equatorial quartz factory. *Earth-Science Reviews*, *197*, 102918. https://doi.org/10.1016/j.earscirev.2019.102918

Garzanti, E., Vezzoli, G., Andò, S., Paparella, P., & Clift, P. D. (2005). Petrology of Indus River sands: A key to interpret erosion history of the Western Himalayan Syntaxis. *Earth and Planetary Science Letters*, *229*(3–4), 287–302. https://doi.org/10.1016/j.epsl.2004.11.008

Gevedon, M., Seman, S., Barnes, J. D., Star, J., & Stockli, D. F. (2018). Unraveling histories of hydrothermal systems via U–Pb laser ablation dating of skarn garnet. *Earth and Planetary Science Letters*, *498*, 237–246. https://doi.org/10.1016/j.epsl.2018.06.036

Glorie, S., Gillespie, J., Simpson, A., Gilbert, S., Khudoley, A., Priyatkina, N., et al. (2022). Detrital apatite Lu–Hf and U–Pb geochronology applied to the southwestern Siberian margin. *Terra Nova*, *34*(3), 201–209. https://doi.org/10.1111/ter.12580

Glorie, S., Hand, M., Mulder, J., Simpson, A., Emo, R. B., Kamber, B., et al. (2023). Robust laser ablation Lu–Hf dating of apatite: An empirical evaluation. *Geological Society, London, Special Publications*, *537*(1). https://doi.org/10.1144/SP537-2022-205

Glorie, S., Mulder, J., Hand, M., Fabris, A., Simpson, A., & Gilbert, S. (2023). Laser ablation (in situ) Lu-Hf dating of magmatic fluorite and hydrothermal fluorite-bearing veins. *Geoscience Frontiers*, *14*(6), 101629. https://doi.org/10.1016/j.gsf.2023.101629

Grew, E. S., Locock, A. J., Mills, S. J., Galuskina, I. O., Galuskin, E. V., & Halenius, U. (2013). Nomenclature of the garnet supergroup. *American Mineralogist*, *98*(4), 785–811. https://doi.org/10.2138/am.2013.4201

Guilmette, C., Smit, M. A., van Hinsbergen, D. J. J., Gürer, D., Corfu, F., Charette, B., et al. (2018). Forced subduction initiation recorded in the sole and crust of the Semail Ophiolite of Oman. *Nature Geoscience*, *11*(9), 688–695. https://doi.org/10.1038/s41561-018-0209-2

Haack, U. K., & Gramse, M. (1972). Survey of garnets for fossil fission tracks. *Contributions to Mineralogy and Petrology*, *34*(3), 258–260. https://doi.org/10.1007/BF00373298

Haack, U. K., & Potts, M. J. (1972). Fission track annealing in garnet. *Contributions to Mineralogy and Petrology*, *34*(4), 343–345. https://doi.org/10.1007/BF00373764

Handy, M. R., Schmid, S. M., Bousquet, R., Kissling, E., & Bernoulli, D. (2010). Reconciling plate-tectonic reconstructions of Alpine Tethys with the geological–geophysical record of spreading and subduction in the Alps. *Earth-Science Reviews*, *102*(3–4), 121–158. https://doi.org/10.1016/j.earscirev.2010.06.002

Handy, M. R., Ustaszewski, K., & Kissling, E. (2015). Reconstructing the Alps–Carpathians–Dinarides as a key to understanding switches in subduction polarity, slab gaps and surface motion. *International Journal of Earth Sciences*, *104*(1), 1–26. https://doi.org/10.1007/s00531-014-1060-3

Hauri, E. H., Wagner, T. P., & Grove, T. L. (1994). Experimental and natural partitioning of Th, U, Pb and other trace elements between garnet, clinopyroxene and basaltic melts. *Chemical Geology*, *117*(1–4), 149–166. https://doi.org/10.1016/0009-2541(94)90126-0

Henrichs, I. A., Chew, D. M., O'Sullivan, G. J., Mark, C., McKenna, C., & Guyett, P. (2019). Trace element (Mn-Sr-Y-Th-REE) and U-Pb isotope systematics of metapelitic apatite during progressive greenschist- to amphibolite-facies Barrovian metamorphism. *Geochemistry, Geophysics, Geosystems*, *20*(8), 4103–4129. https://doi.org/10.1029/2019GC008359

Hubert, J. (1962). A zircon-tourmaline-rutile maturity index and the interdependence of the composition of heavy mineral assemblages with the gross composition and texture of sandstones. *SEPM Journal of Sedimentary Research*, *32*(3), 440–450. https://doi.org/10.1306/74D70CE5-2B21-11D7-8648000102C1865D

Iolite. [Software]. Retrieved from www.iolite.xyz

Janots, E., Engi, M., Rubatto, D., Berger, A., Gregory, C., & Rahn, M. (2009). Metamorphic rates in collisional orogeny from in situ allanite and monazite dating. *Geology*, *37*(1), 11–14. https://doi.org/10.1130/G25192A.1

Jochum, K. P., Stoll, B., Herwig, K., Willbold, M., Hofmann, A. W., Amini, M., et al. (2006). MPI-DING reference glasses for in situ microanalysis: New reference values for element concentrations and isotope ratios. *Geochemistry, Geophysics, Geosystems*, *7*(2), Q02008. https://doi.org/10.1029/2005GC001060

Jollands, M. C., O'Neill, H. S. C., & Hermann, J. (2014). The importance of defining chemical potentials, substitution mechanisms and solubility in trace element diffusion studies: The case of Zr and Hf in olivine. *Contributions to Mineralogy and Petrology*, *168*(3), 1–19. https://doi.org/10.1007/s00410-014-1055-x

Kennan, P. S., & Murphy, F. C. (1993). Coticule in lower Ordovician metasediments near the hidden Kentstown granite, county Meath. *Irish Journal of Earth Sciences*, *12*, 41–46.

Kohn, M. J. (2009). Models of garnet differential geochronology. *Geochimica et Cosmochimica Acta*, *73*(1), 170–182. https://doi.org/10.1016/j.gca.2008.10.004

Kohn, M. J. (2014). "Thermoba-Raman-try": Calibration of spectroscopic barometers and thermometers for mineral inclusions. *Earth and Planetary Science Letters*, *388*, 187–196. https://doi.org/10.1016/j.epsl.2013.11.054

Kooijman, E., Mezger, K., & Berndt, J. (2010). Constraints on the U–Pb systematics of metamorphic rutile from in situ LA-ICP-MS analysis. *Earth and Planetary Science Letters*, *293*(3–4), 321–330. https://doi.org/10.1016/j.epsl.2010.02.047

LADR. [Software]. Norris Scientific. Retrieved from www.norsci.com

Ledent, D., Patterson, C., & Tilton, G. R. (1964). Ages of zircon and feldspar concentrates from North American beach and river sands. *The Journal of Geology*, *72*(1), 112–122. https://doi.org/10.1086/626967

Liati, A., Gebauer, D., & Fanning, C. M. (2009). Geochronological evolution of HP metamorphic rocks of the Adula nappe, Central Alps, in pre-Alpine and Alpine subduction cycles. *Journal of the Geological Society*, *166*(4), 797–810. https://doi.org/10.1144/0016-76492008-033

Ludwig, K. R. (2012). *User's manual for Isoplot 3.75: A geochronological toolkit for Microsoft Excel* (Vol. 4, p. 70). Berkeley Geochronology Center Special Publication.

Machado, N., & Gauthier, G. (1996). Determination of $^{207}Pb/^{206}Pb$ ages on zircon and monazite by laser-ablation ICPMS and application to a study of sedimentary provenance and metamorphism in southeastern Brazil. *Geochimica et Cosmochimica Acta*, *60*(24), 5063–5073. https://doi.org/10.1016/S0016-7037(96)00287-6

Malinovsky, D., Stenberg, A., Rodushkin, I., Andren, H., Ingri, J., Öhlander, B., & Baxter, D. C. (2003). Performance of high resolution MC-ICP-MS for Fe isotope ratio measurements in sedimentary geological materials. *Journal of Analytical Atomic Spectrometry*, *18*(7), 687–695. https://doi.org/10.1039/b302312e

Malusà, M. G., Wang, J., Garzanti, E., Liu, Z., Villa, I. M., & Wittmann, H. (2017). Trace-element and Nd-isotope systematics in detrital apatite of the Po river catchment: Implications for provenance discrimination and the lag-time approach to detrital thermochronology. *Lithos*, *290–291*, 48–59. https://doi.org/10.1016/j.lithos.2017.08.006

Maneiro, K. A., Baxter, E. F., Samson, S. D., Marschall, H. R., & Hietpas, J. (2019). Detrital garnet geochronology: Application in tributaries of the French broad river, southern Appalachian Mountains, USA. *Geology*, *47*(12), 1189–1192. https://doi.org/10.1130/G46840.1

Mange, M. A., & Otvos, E. G. (2005). Gulf coastal plain evolution in West Louisiana: Heavy mineral provenance and Pleistocene alluvial chronology. *Sedimentary Geology*, *182*(1–4), 29–57. https://doi.org/10.1016/j.sedgeo.2005.07.015

Manzotti, P., & Ballèvre, M. (2013). Multistage garnet in high-pressure metasediments: Alpine overgrowths on Variscan detrital grains. *Geology*, *41*(11), 1151–1154. https://doi.org/10.1130/G34741.1

Mark, C., Cogné, N., & Chew, D. (2016). Tracking exhumation and drainage divide migration of the Western Alps: A test of the apatite U-Pb thermochronometer as a detrital provenance tool. *Bulletin of the Geological Society of America*, *128*(9–10), 1439–1460. https://doi.org/10.1130/B31351.1

Mark, C., Cogné, N., Chew, D., & Henrichs, I. (2018). Detecting orogenic wedge state and the rise of the External Alps by detrital thermochronology. *EarthArXiv*. https://doi.org/10.31223/osf.io/d36xz

Mark, C., O'Sullivan, G., Glorie, S., Simpson, A., Andò, S., Barbarano, M., et al. (2023). Detrital garnet geochronology by in-situ U-Pb and Lu-Hf analysis: A case study from the European Alps [Dataset]. Zenodo. https://doi.org/10.5281/zenodo.7900189

Matte, P. (2001). The Variscan collage and orogeny (480–290 Ma) and the tectonic definition of the Armorica microplate: A review. *Terra Nova*, *13*(2), 122–128. https://doi.org/10.1046/j.1365-3121.2001.00327.x

Mezger, K., Hanson, G. N., & Bohlen, S. R. (1989). U-Pb systematics of garnet: Dating the growth of garnet in the Late Archean Pikwitonei granulite domain at Cauchon and Natawahunan Lakes, Manitoba, Canada. *Contributions to Mineralogy and Petrology*, *101*(2), 136–148. https://doi.org/10.1007/BF00375301

Milliken, K. L. (2007). Chapter 8 Provenance and diagenesis of heavy minerals, Cenozoic units of the northwestern Gulf of Mexico sedimentary basin. *Developments in Sedimentology*, 247–261. https://doi.org/10.1016/S0070-4571(07)58008-8

Millonig, L. J., Albert, R., Gerdes, A., Avigad, D., & Dietsch, C. (2020). Exploring laser ablation U–Pb dating of regional metamorphic garnet – The Straits Schist, Connecticut, USA. *Earth and Planetary Science Letters*, *552*, 116589. https://doi.org/10.1016/j.epsl.2020.116589

Moecher, D., & Samson, S. D. (2006). Differential zircon fertility of source terranes and natural bias in the detrital zircon record: Implications for sedimentary provenance analysis. *Earth and Planetary Science Letters*, *247*(3–4), 252–266. https://doi.org/10.1016/j.epsl.2006.04.035

Morton, A. C. (1985). A new approach to provenance studies: Electron microprobe analysis of detrital garnets from Middle Jurassic sandstones of the northern North Sea. *Sedimentology*, *32*(4), 553–566. https://doi.org/10.1111/j.1365-3091.1985.tb00470.x

Morton, A. C., & Hallsworth, C. (2007). Stability of detrital heavy minerals during burial diagenesis. In M. Mange & D. Wright (Eds.), *Developments in Sedimentology* (Vol. 58, pp. 215–245). Elsevier. https://doi.org/10.1016/S0070-4571(07)58007-6

Najman, Y. (2006). The detrital record of orogenesis: A review of approaches and techniques used in the Himalayan sedimentary basins. *Earth-Science Reviews*, *74*(1–2), 1–72. https://doi.org/10.1016/j.earscirev.2005.04.004

Nebel, O., Morel, M. L. A., & Vroon, P. Z. (2009). Isotope dilution determinations of Lu, Hf, Zr, Ta and W, and Hf isotope compositions of NIST SRM 610 and 612 glass wafers. *Geostandards and Geoanalytical Research*, *33*(4), 487–499. https://doi.org/10.1111/j.1751-908X.2009.00032.x

Nicolaysen, L. O. (1961). Graphic interpretation of discordant age measurements on metamorphic rocks. *Annals of the New York Academy of Sciences*, *91*(2), 198–206. https://doi.org/10.1111/j.1749-6632.1961.tb35452.x

Oliver, G. J. H., Chen, F., Buchwaldt, R., & Hegner, E. (2000). Fast tectonometamorphism and exhumation in the type area of the Barrovian and Buchan zones. *Geology*, *28*(5), 459. https://doi.org/10.1130/0091-7613(2000)28<459:FTAEIT>2.0.CO;2

O'Sullivan, G. J., Hoare, B. C., Mark, C., Drakou, F., & Tomlinson, E. L. (2023). Uranium–lead geochronology applied to pyrope garnet with very low concentrations of uranium. *Geological Magazine*, *160*(5), 1–10. https://doi.org/10.1017/S0016756823000122

Paton, C., Hellstrom, J., Paul, B., Woodhead, J., & Hergt, J. (2011). Iolite: Freeware for the visualisation and processing of mass spectrometric data. *Journal of Analytical Atomic Spectrometry*, *26*(12), 2508. https://doi.org/10.1039/c1ja10172b

Raimondo, T., Payne, J., Wade, B., Lanari, P., Clark, C., & Hand, M. (2017). Trace element mapping by LA-ICP-MS: Assessing geochemical mobility in garnet. *Contributions to Mineralogy and Petrology*, *172*(4), 1–22. https://doi.org/10.1007/s00410-017-1339-z

Rak, Z., Ewing, R., & Becker, U. (2011). Role of iron in the incorporation of uranium in ferric garnet matrices. *Physical Review B*, *84*(15), 155128-1–155128-10. https://doi.org/10.1103/PhysRevB.84.155128

Romer, R., & Smeds, S.-A. (1996). U-Pb columbite ages of pegmatites from Sveconorwegian terranes in southwestern Sweden. *Precambrian Research*, *76*(1–2), 15–30. https://doi.org/10.1016/0301-9268(95)00023-2

Rubatto, D., & Hermann, J. (2003). Zircon formation during fluid circulation in eclogites (Monviso, Western Alps): Implications for Zr and Hf budget in subduction zones. *Geochimica et Cosmochimica Acta*, *67*(12), 2173–2187. https://doi.org/10.1016/S0016-7037(02)01321-2

Salnikova, E., Chakhmouradian, A. R., Stifeeva, M. V., Reguir, E. P., Kotov, A. B., Gritsenko, Y. D., & Nikiforov, A. V. (2019). Calcic garnets as a geochronological and petrogenetic tool applicable to a wide variety of rocks. *Lithos*, *338–339*, 141–154. https://doi.org/10.1016/j.lithos.2019.03.032

Salnikova, E., Stifeeva, M. V., Nikiforov, A. V., Yarmolyuk, A. V. V., Kotov, A. B., Anisimova, I. V., et al. (2018). Andradite–Morimotoite garnets as promising U–Pb geochronometers for dating ultrabasic alkaline rocks. *Doklady Earth Sciences*, *480*(5), 778–782. https://doi.org/10.1134/S1028334X18060168

Schlunegger, F., Burbank, D. W., Matter, A., Engesser, B., & Mödden, C. (1996). Magnetostratigraphic calibration of the Oligocence to Middle Miocene (30–15 Ma) mammal biozones and depositional sequences of the Swiss Molasse Basin. *Eclogae Geologicae Helvetiae*, *89*, 753–788.

Schmid, S. M., Bernoulli, D., Fügenschuh, B., Matenco, L., Schefer, S., Schuster, R., et al. (2008). The Alpine-Carpathian-Dinaridic orogenic system: Correlation and evolution of tectonic units. *Swiss Journal of Geosciences*, *101*(1), 139–183. https://doi.org/10.1007/s00015-008-1247-3

Schönig, J., von Eynatten, H., Tolosana-Delgado, R., & Meinhold, G. (2021). Garnet major-element composition as an indicator of host-rock type: A machine learning approach using the random forest classifier. *Contributions to Mineralogy and Petrology*, *176*(12), 98. https://doi.org/10.1007/s00410-021-01854-w

Schulz, B., & von Raumer, J. F. (2011). Discovery of Ordovician-Silurian metamorphic monazite in garnet metapelites of the Alpine External Aiguilles Rouges Massif. *Swiss Journal of Geosciences*, *104*(1), 67–79. https://doi.org/10.1007/s00015-010-0048-7

Schuster, R., & Stüwe, K. (2008). Permian metamorphic event in the Alps. *Geology*, *36*(8), 603–606. https://doi.org/10.1130/G24703A.1

Seman, S., Stockli, D. F., & Mclean, N. M. (2017). U-Pb geochronology of grossular-andradite garnet. *Chemical Geology*, *460*, 106–116. https://doi.org/10.1016/j.chemgeo.2017.04.020

Simpson, A., Gilbert, S., Tamblyn, R., Hand, M., Spandler, C., Gillespie, J., et al. (2021). In-situ Lu–Hf geochronology of garnet, apatite and xenotime by LA ICP MS/MS. *Chemical Geology*, *577*, 120299. https://doi.org/10.1016/j.chemgeo.2021.120299

Simpson, A., Glorie, S., Hand, M., Spandler, C., & Gilbert, S. (2023). Garnet Lu-Hf speed dating: A novel method to rapidly resolve polymetamorphic histories. *Gondwana Research*, *121*, 215–234. https://doi.org/10.1016/j.gr.2023.04.011

Simpson, A., Glorie, S., Hand, M., Spandler, C., Gilbert, S., & Cave, B. (2022). In situ Lu-Hf geochronology of calcite. *Geochronology*, *4*(1), 353–372. https://doi.org/10.5194/gchron-4-353-2022

Smit, M. A., Scherer, E. E., & Mezger, K. (2013). Lu-Hf and Sm-Nd garnet geochronology: Chronometric closure and implications for dating petrological processes. *Earth and Planetary Science Letters*, *381*, 222–233. https://doi.org/10.1016/j.epsl.2013.08.046

Smith, M. P., Henderson, P., Jeffries, T. E. R., Long, J., & Williams, C. T. (2004). The rare earth elements and uranium in garnets from the Beinn an Dubhaich aureole, Skye, Scotland, UK: Constraints on processes in a dynamic hydrothermal system. *Journal of Petrology*, *45*(3), 457–484. https://doi.org/10.1093/petrology/egg087

Spencer, C. J., Kirkland, C. L., Roberts, N. M. W., Evans, N. J., & Liebmann, J. (2020). Strategies towards robust interpretations of in situ zircon Lu–Hf isotope analyses. *Geoscience Frontiers*, *11*(3), 843–853. https://doi.org/10.1016/j.gsf.2019.09.004

Stacey, J. S., & Kramers, J. D. (1975). Approximation of terrestrial lead isotope evolution by a two-stage model. *Earth and Planetary Science Letters*, *26*(2), 207–221. https://doi.org/10.1016/0012-821X(75)90088-6

Stampfli, G. M., & Hochard, C. (2009). Plate tectonics of the Alpine realm. *Geological Society, London, Special Publications*, *327*(1), 89–111. https://doi.org/10.1144/SP327.6

Stifeeva, M. V., Salnikova, E. B., Samsonov, A. V., Kotov, A. B., & Gritsenko, Y. D. (2019). Garnet U–Pb age of skarns from Dashkesan deposit (Lesser Caucasus). *Doklady Earth Sciences*, *487*(2), 953–956. https://doi.org/10.1134/S1028334X19080178

Stutenbecker, L., Berger, A., & Schlunegger, F. (2017). The potential of detrital garnet as a provenance proxy in the Central Swiss Alps. *Sedimentary Geology*, *351*, 11–20. https://doi.org/10.1016/j.sedgeo.2017.02.002

Stutenbecker, L., Tollan, P. M. E., Madella, A., & Lanari, P. (2019). Miocene basement exhumation in the Central Alps recorded by detrital garnet geochemistry in foreland basin deposits. *Solid Earth*, *10*(5), 1581–1595. https://doi.org/10.5194/se-10-1581-2019

Suggate, S. M., & Hall, R. (2014). Using detrital garnet compositions to determine provenance: A new compositional database and procedure. *Geological Society Special Publication*, *386*(1), 373–393. https://doi.org/10.1144/SP386.8

Thöni, M. (2003). Sm–Nd isotope systematics in garnet from different lithologies (Eastern Alps): Age results, and an evaluation of potential problems for garnet Sm–Nd chronometry. *Chemical Geology*, *194*(4), 353–379. https://doi.org/10.1016/S0009-2541(02)00419-9

Van Westrenen, W., Blundy, J., & Wood, B. (1999). Crystal-chemical controls on trace element partitioning between garnet and anhydrous silicate melt. *American Mineralogist*, *84*(5–6), 838–847. https://doi.org/10.2138/am-1999-5-617

Velbel, M. A. (1984). Natural weathering mechanisms of almandine garnet. *Geology*, *12*(10), 631–634. https://doi.org/10.1130/0091-7613(1984)12<631:NWMOAG>2.0.CO;2

Vermeesch, P. (2012). On the visualisation of detrital age distributions. *Chemical Geology*, *312–313*, 190–194. https://doi.org/10.1016/j.chemgeo.2012.04.021

Vermeesch, P. (2018). IsoplotR: A free and open toolbox for geochronology. *Geoscience Frontiers*, *9*(5), 1479–1493. https://doi.org/10.1016/j.gsf.2018.04.001

Vervoort, J. D., Patchett, P. J., Blichert-Toft, J., & Albarède, F. (1999). Relationships between Lu-Hf and Sm-Nd isotopic systems in the global sedimentary system. *Earth and Planetary Science Letters*, *168*(1–2), 79–99. https://doi.org/10.1016/s0012-821x(99)00047-3

von Eynatten, H., & Dunkl, I. (2012). Assessing the sediment factory: The role of single grain analysis. *Earth-Science Reviews*, *115*(1–2), 97–120. https://doi.org/10.1016/j.earscirev.2012.08.001

von Raumer, J. F., Bussy, F., & Stampfli, G. M. (2009). The Variscan evolution in the External massifs of the Alps and place in their Variscan framework. *Comptes Rendus Geoscience*, *341*(2–3), 239–252. https://doi.org/10.1016/j.crte.2008.11.007

Walker, S., Bird, A. F., Thirlwall, M. F., & Strachan, R. A. (2021). Caledonian and pre-Caledonian orogenic events in Shetland, Scotland: Evidence from garnet Lu–Hf and Sm–Nd geochronology. *Geological Society, London, Special Publications*, *503*(1), 305–331. https://doi.org/10.1144/SP503-2020-32

White, R. W., Powell, R., & Johnson, T. E. (2014). The effect of Mn on mineral stability in metapelites revisited: New A-X relations for manganese-bearing minerals. *Journal of Metamorphic Geology*, *32*(8), 809–828. https://doi.org/10.1111/jmg.12095

Woods, G. (2016). *Resolution of ^{176}Yb and ^{176}Lu interferences on ^{176}Hf to enable accurate ^{176}Hf/^{177}Hf isotope ratio analysis using an Agilent 8800 ICP-QQQ with MS/MS* (Technical Note). Agilent Technologies, Inc. https://doi.org/10.13140/RG.2.1.3971.6245

Yang, Y. H., Wu, F. Y., Yang, J. H., Mitchell, R. H., Zhao, Z. F., Xie, L. W., et al. (2018). U-Pb age determination of schorlomite garnet by laser ablation inductively coupled plasma mass spectrometry. *Journal of Analytical Atomic Spectrometry*, *33*(2), 231–239. https://doi.org/10.1039/c7ja00315c

Zack, T., Stockli, D. F., Luvizotto, G. L., Barth, M. G., Belousova, E., Wolfe, M. R., & Hinton, R. W. (2011). In situ U-Pb rutile dating by LA-ICP-MS: ^{208}Pb correction and prospects for geological applications. *Contributions to Mineralogy and Petrology*, *162*(3), 515–530. https://doi.org/10.1007/s00410-011-0609-4

Zhao, Z. F., & Zheng, Y. F. (2007). Diffusion compensation for argon, hydrogen, lead, and strontium in minerals: Empirical relationships to crystal chemistry. In *American Mineralogist* (Vol. 92, pp. 289–308). Mineralogical Society of America. https://doi.org/10.2138/am.2007.2127

Zimmermann, S., Mark, C., Chew, D., & Voice, P. J. (2018). Maximising data and precision from detrital zircon U-Pb analysis by LA-ICPMS: The use of core-rim ages and the single-analysis concordia age. *Sedimentary Geology*, *375*, 5–13. https://doi.org/10.1016/j.sedgeo.2017.12.020